NAVAL POSTGRADUATE SCHOOL

MONTEREY, CALIFORNIA

THESIS

EXPERIMENTS ON LASER BEAM JITTER CONTROL WITH APPLICATIONS TO A SHIPBOARD FREE ELECTRON LASER

by

Brett E. Bateman

December 2007

Thesis Advisor:	Steven R. Baker
Thesis Co-Adviser:	Brij N. Agrawal
Second Reader:	Hyungjoon Yoon

THIS PAGE INTENTIONALLY LEFT BLANK

REPORT DOCUMENTATION PAGE			Form Approved OMB No. 0704-0188
Public reporting burden for this collection of information is estimated to average 1 hour per response, including the time for reviewing instruction, searching existing data sources, gathering and maintaining the data needed, and completing and reviewing the collection of information. Send comments regarding this burden estimate or any other aspect of this collection of information, including suggestions for reducing this burden, to Washington headquarters Services, Directorate for Information Operations and Reports, 1215 Jefferson Davis Highway, Suite 1204, Arlington, VA 22202-4302, and to the Office of Management and Budget, Paperwork Reduction Project (0704-0188) Washington DC 20503.			
1. AGENCY USE ONLY *(Leave blank)*	**2. REPORT DATE** December 2007	**3. REPORT TYPE AND DATES COVERED** Master's Thesis	
4. TITLE AND SUBTITLE Experiments on Laser Beam Jitter Control with Applications to a Shipboard Free Electron Laser		**5. FUNDING NUMBERS**	
6. AUTHOR(S) Brett Bateman			
7. PERFORMING ORGANIZATION NAME(S) AND ADDRESS(ES) Naval Postgraduate School Monterey, CA 93943-5000		**8. PERFORMING ORGANIZATION REPORT NUMBER**	
9. SPONSORING /MONITORING AGENCY NAME(S) AND ADDRESS(ES) N/A		**10. SPONSORING/MONITORING AGENCY REPORT NUMBER**	
11. SUPPLEMENTARY NOTES The views expressed in this thesis are those of the author and do not reflect the official policy or position of the Department of Defense or the U.S. Government.			
12a. DISTRIBUTION / AVAILABILITY STATEMENT Approved for public release; distribution is unlimited		**12b. DISTRIBUTION CODE**	

13. ABSTRACT (maximum 200 words)

A Free Electron Laser (FEL) shows potential as an effective defensive weapon for a naval ship against today's modern weapons such as supersonic anti-ship missiles. A laser can destroy these fast and highly maneuverable missiles at the speed of light. Several obstacles must be overcome to employ this weapon on a naval ship. This thesis discusses several methods for passive and active jitter control of a guided optical beam which might be employed in a FEL weapon system.

Vibration experiments were performed on the Laser Jitter Control Testbed at the Naval Postgraduate School to test several types of feedback and adaptive feedforward controllers. A Filtered-X Recursive Least Squares (FXRLS) adaptive feedforward controller was found to be most effective to correct a combination of both broadband and narrowband disturbances. The FXRLS controller results in a 33 dB decrease in jitter caused by a 50 Hz narrowband vibration and an 89% improvement in low frequency broadband jitter experienced by the optical beam. A proposed Free Electron Laser design employing both passive and active vibration control techniques is recommended that employs a co-linear optical reference beam for jitter control.

14. SUBJECT TERMS Adaptive Control, Optical Beam, Jitter, Recursive Least Squares			**15. NUMBER OF PAGES** 99
			16. PRICE CODE
17. SECURITY CLASSIFICATION OF REPORT Unclassified	**18. SECURITY CLASSIFICATION OF THIS PAGE** Unclassified	**19. SECURITY CLASSIFICATION OF ABSTRACT** Unclassified	**20. LIMITATION OF ABSTRACT** UU

NSN 7540-01-280-5500 Standard Form 298 (Rev. 2-89)
Prescribed by ANSI Std. 239-18

THIS PAGE INTENTIONALLY LEFT BLANK

Approved for public release; distribution is unlimited

EXPERIMENTS ON LASER BEAM JITTER CONTROL WITH APPLICATIONS TO A SHIPBOARD FREE ELECTRON LASER

Brett E. Bateman
Lieutenant, United States Navy
B.S., United States Naval Academy, 2001

Submitted in partial fulfillment of the
requirements for the degree of

MASTER OF SCIENCE IN APPLIED PHYSICS

from the

NAVAL POSTGRADUATE SCHOOL
December 2007

Author: Brett E. Bateman

Approved by: Steven R. Baker
Thesis Advisor

Brij N. Agrawal
Co-Advisor

Hyungjoon Yoon
Second Reader

James H. Luscombe
Chairman, Department of Physics

THIS PAGE INTENTIONALLY LEFT BLANK

ABSTRACT

A Free Electron Laser (FEL) shows potential as an effective defensive weapon for a naval ship against today's modern weapons such as supersonic anti-ship missiles. A laser can destroy these fast and highly maneuverable missiles at the speed of light. Several obstacles must be overcome to employ this weapon on a naval ship. This thesis discusses several methods for passive and active jitter control of a guided optical beam which might be employed in a FEL weapon system.

Vibration experiments were performed on the Laser Jitter Control Testbed at the Naval Postgraduate School to test several types of feedback and adaptive feedforward controllers. A Filtered-X Recursive Least Squares (FXRLS) adaptive feedforward controller was found to be most effective to correct a combination of both broadband and narrowband disturbances. The FXRLS controller results in a 33 dB decrease in jitter caused by a 50 Hz narrowband vibration and an 89% improvement in low frequency broadband jitter experienced by the optical beam. A proposed Free Electron Laser design employing both passive and active vibration control techniques is recommended that employs a co-linear optical reference beam for jitter control.

THIS PAGE INTENTIONALLY LEFT BLANK

TABLE OF CONTENTS

I. INTRODUCTION....1

II. VIBRATION ISSUES FOR A SHIPBOARD FREE ELECTRON LASER....3
- **A. DESCRIPTION OF PROPOSED FREE ELECTRON LASER....3**
  - **1. Electron Beam....3**
  - **2. Optical Beam....4**
- **B. VIBRATION ENVIRONMENT FOR A SHIPBOARD FREE ELECTRON LASER....5**
- **C. VIBRATION LIMITS FOR A FREE ELECTRON LASER....7**
  - **1. Postulated Limits from Computer Modeling....7**
  - **2. Measured Vibration on a Functioning Free Electron Laser and in a Laboratory....7**
    - ***a. Test Equipment for Measurement of Vibration....8***
    - ***b. Accelerometer Mounting Locations....8***
    - ***c. Results of Accelerometer Measurements....9***
  - **3. Discussion of Vibration Limits....11**

III. REVIEW OF VIBRATION CONTROL THEORY....13
- **A. PASSIVE VIBRATION ISOLATION....13**
  - **1. Single Stage Isolation....13**
  - **2. Two Stage Isolation....16**
- **B. ACTIVE VIBRATION ISOLATION....17**
  - **1. Fixed Feedback....18**
    - ***a. Linear Quadratic Regulators....18***
  - **2. Adaptive Feedback....20**
  - **3. Adaptive Feedforward....21**
    - ***a. The Least Mean Square Algorithm....23***
    - ***b. Recursive Least Square Algorithm....25***

IV. EXPERIMENTAL SETUP....29
- **A. LASER JITTER CONTROL TESTBED....29**
- **B. DETECTORS....31**
- **C. FAST STEERING MIRRORS....32**
  - **1. Disturbance Mirror – Baker Fast Steering Mirror....32**
  - **2. Control Mirror-Newport Fast Steering Mirror....33**
- **D. INERTIAL ACTUATOR....34**
- **E. VIBRATION ISOLATION PLATFORMS....34**
  - **1. Newport Optical Table....34**
  - **2. Newport Vibration Isolation Platform....35**
- **F. COMPUTER CONTROL SYSTEM AND SOFTWARE....36**

V. SYSTEM IDENTIFICATION EXPERIMENTS....37
- **A. NON-PARAMETRIC FREQUENCY DOMAIN METHOD....37**
- **B. PARAMETER ESTIMATION METHOD....38**

1. Experimental Results of System Identification 38

VI. DISTURBANCE REJECTION EXPERIMENTS ON THE LJC TESTBED 43
A. LQG CONTROLLER 44
B. DISTURBANCE REJECTION EXPERIMENTS 44
1. Case 1: Small Broadband Disturbance from DFSM 44
2. Case 2: Large Broadband Disturbance from DFSM 47
3. Case 3: Narrowband Disturbance from DFSM 49
4. Case 4: Narrowband and Broadband Disturbance from DFSM 52

VII. DESIGN RECOMMENDATIONS FOR FREE ELECTRON LASER WEAPON SYSTEM VIBRATION CONTROL 55
A. EXAMPLE VIBRATION CONTROL OF AN OPTICAL BEAM SYSTEM – THE AIRBORNE LASER 55
B. COMPARISON OF AIRBORNE LASER AND FREE ELECTRON LASER DESIGN 58
C. DESIGN RECOMMENDATIONS FOR THE VIBRATION CONTROL OF AN FEL ON A SHIP 59

VIII. CONCLUSIONS 63
A. SUMMARY OF RESULTS 63
B. CONCLUSIONS 64
C. SUGGESTIONS FOR FOLLOW-ON RESEARCH 64

APPENDIX A: TRIAXIAL ACCELEROMETER CALIBRATION CERTIFICATES 67

APPENDIX B: SAMPLE MATLAB CODE FOR CALCULATION OF DISPLACEMENT FOR LINEAR ACCELEROMETERS 69

APPENDIX C: EQUIPMENT SPECIFICATIONS 71
A. ON-TRAK POSITION SENSING DETECTOR 71
B. BAKER STEERING MIRROR 73
C. NEWPORT FAST STEERING MIRROR 74

APPENDIX D: SOFTWARE VERSIONS 75

APPENDIX E: SYSTEM IDENTIFICATION CODE 77

APPENDIX F: LQG AND KALMAN ESTIMATOR CALCULATIONS 79

LIST OF REFERENCES 81

INITIAL DISTRIBUTION LIST 83

LIST OF FIGURES

Figure 1 Free Electron Laser System Diagram. From [Allgaier 3] 3
Figure 2 Undulator Schematic. 4
Figure 3 Displacement Measured from Accelerometer 11
Figure 4 Passive Vibration Mounting. After [Newport] 13
Figure 5 Transmissibility of a Simple Mass-Spring-Damper System. After [Beranek and Ver 560] 15
Figure 6 Two-Stage Isolation 16
Figure 7 Transmissibility of Two-Stage System. From [Beranek and Ver 574] 17
Figure 8 Full State Feedback Controller in Discrete Time 19
Figure 9 Full State Feedback Controller with an Integrator 20
Figure 10 Single-channel Feedback ANC System. From [Kuo 12] 21
Figure 11 Single-channel Broadband Feedforward ANC System in a Duct. From [Kuo 10] 21
Figure 12 Block Diagram of an ANC system. After [Kuo 59] 22
Figure 13 Transversal Filter. From [Kuo 18] 23
Figure 14 MSE Surface. From[Kuo 21] 24
Figure 15 FXLMS Diagram. From [Kuo 64] 25
Figure 16 FXRLS Diagram. From [Kuo 264] 28
Figure 17 Laser Jitter Control Testbed 29
Figure 18 Laser Jitter Control Testbed 30
Figure 19 Position Sensing Module 31
Figure 20 Baker Fast Steering Mirror 32
Figure 21 Newport Fast Steering Mirror 33
Figure 22 CSA Engineering Inertial Actuator 34
Figure 23 Newport I-2000 Pneumatic Isolator. From [Newport] 35
Figure 24 Newport Vibration Isolation Frequency Response. From [Newport] 35
Figure 25 Signal Flow Diagram. After [Watkins 35] 36
Figure 26 Frequency Response of Open-Loop System Y-Axis 40
Figure 27 Frequency Response of Open-Loop System X-Axis 41
Figure 28 X Axis PSD Case 1, Small Broadband Disturbance 45
Figure 29 Y Axis PSD Case 1, Small Broadband Disturbance 45
Figure 30 Mean Square Error Case 1, Small Broadband Disturbance 46
Figure 31 X Axis PSD Case 2, Large Broadband Disturbance 47
Figure 32 Y Axis PSD Case 2, Large Broadband Disturbance 48
Figure 33 MSE Case 2, Large Broadband Disturbance 48
Figure 34 X Axis PSD Case 3, Narrowband Disturbance 50
Figure 35 Y Axis PSD Case 3, Narrowband Disturbance 50
Figure 36 MSE Case 3, Narrowband Disturbance 51
Figure 37 X Axis PSD Case 4, BB and NB Disturbance 52
Figure 38 Y Axis PSD Case 4, BB and NB Disturbance 52
Figure 39 MSE Case 4, NB and BB Disturbance 53
Figure 40 ABL Beam Train. From [Kenchner 12] 56

Figure 41 ABL Component Diagram. From [Glaese 152].....56
Figure 42 ABL Jitter Control Architecture. From [Kelchner 12] 57
Figure 43 Triaxial Accelerometer Calibration Certificates.....67
Figure 44 On-Trak Position Sensing Module Diagram. From ["Position Sensing Modules"] 71
Figure 45 On-Trak Typical Operating Circuit. From ["Position Sensing Modules"].....71
Figure 46 Baker Fast Steering Mirror Specifications. From [Watkins 131] 73
Figure 47 Newport Fast Steering Mirror Specifications. From [Watkins 129].....74

LIST OF TABLES

Table 1. FFG-7 Maximum Amplitude, Minimum Period Motions. From [Allen 28] 5
Table 2. MIL-STD-167-1A Variable Frequency Test Requirements. 6
Table 3. Case 1 Results, Small Broadband Disturbance 46
Table 4. Case 2 Results, Large Broadband Disturbance 49
Table 5. Case 3 Results, Narrowband Disturbance 51
Table 6. Case 4 Results, NB and BB Disturbance 53
Table 7. On-Trak Position Sensing Detector Specifications. After ["Position Sensing Modules"] 71
Table 8. Software Versions 75

THIS PAGE INTENTIONALLY LEFT BLANK

ACKNOWLEDGMENTS

I would like to thank my wife Kathleen, daughter Anna, and son Ian for their encouragement and prayers on my behalf. They have been so supportive of my naval career.

I thank Professor Baker for providing excellent instruction in vibration control and assisting in the actual data analysis. Professor Agrawal provided me the opportunity to use the advanced and modern test equipment in the Space Research and Design Center. Professor Colson and the Free Electron Laser research team were a great help in understanding the basics of the Free Electron Laser. Professor Todd Smith at Stanford University provided access to take vibration measurements on Stanford's Free Electron Laser. I would also like to thank Dr. Drake Yoon for his guidance on control theory and assistance on applying the theory to the testbed, and for taking the time to meet with me nearly daily. Dr. David Kienholz of CSA Engineering provided helpful insight into important vibration design aspects for putting the Free Electron Laser on a ship and into what has been done on the Airborne Laser program. I would like to thank fellow student Mr. Matt Allen for his assistance in getting me up to speed on modern control theory and on how to use the Laser Jitter Control Testbed control system.

THIS PAGE INTENTIONALLY LEFT BLANK

I. INTRODUCTION

A Free Electron Laser (FEL) on a naval ship has tremendous potential for missile defense of the ship against modern weapons such as supersonic anti-ship missiles. Modern missiles can perform quick high g turns at incredible speeds. A laser can destroy these fast and highly maneuverable missiles at the speed of light. Another advantage of a Free Electron Laser is the ability to tune the wavelength of the high energy beam to minimize the effect of atmospheric disturbances.

Several obstacles must be overcome to employ this weapon on a naval ship. This thesis discusses the effects of vibration on the Free Electron Laser and proposes several methods for passive and active jitter control of the laser beam.

Chapter II provides a background on the alignments issues of a Free Electron Laser and discusses the vibration levels expected on a ship.

Chapter III is a review of passive vibration control and modern control theory. It explores fixed feedback, adaptive feedback, and adaptive feedforward control techniques.

Chapter IV describes the experimental set-up of the Laser Jitter Control Testbed in the Space Research and Design Center at the Naval Postgraduate School.

Chapter V explains modern system identification techniques and derives the system identification models used on the Laser Jitter Control Testbed.

Chapter VI includes the results of disturbance rejection experiments for four different types of disturbances.

Chapter VII covers vibration control techniques used on the U.S. Air Force's Airborne Laser. It discusses design recommendations for vibration control of a Free Electron Laser on a ship.

THIS PAGE INTENTIONALLY LEFT BLANK

II. VIBRATION ISSUES FOR A SHIPBOARD FREE ELECTRON LASER

A. DESCRIPTION OF PROPOSED FREE ELECTRON LASER

A Free Electron Laser (FEL) creates tunable coherent electromagnetic radiation by sending accelerated free relativistic electrons through a transverse and periodic magnetic field. The following description will explain the interaction of the electron and optical beams with their associated components. Figure 1 shows the major components of the FEL. The red line represents the electron beam. The blue line is the optical beam.

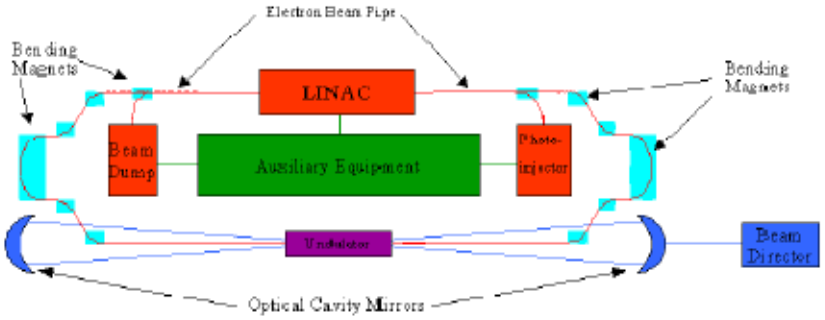

Figure 1 Free Electron Laser System Diagram. From [Allgaier 3]

1. Electron Beam

The electron injector creates free electrons that are sent to the electron accelerator. The electrons leave the accelerator at high energies before being guided to the undulator using a series of adjustable magnets. The relativistic free electrons emit radiation as they oscillate through the periodic transverse magnetic field of the undulator, or otherwise called wiggler, as shown in Figure 2 below. The electrons can then be recycled to conserve energy by recirculating the electron beam.

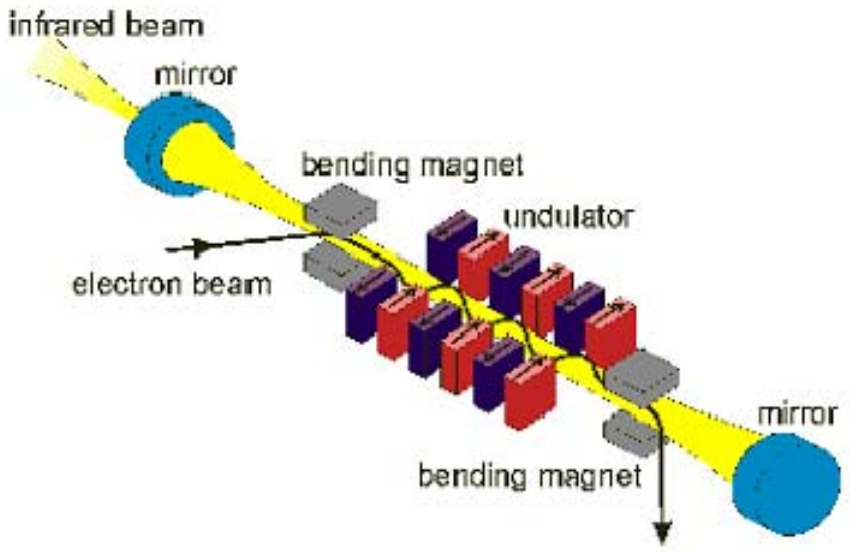

Figure 2 Undulator Schematic.

2. Optical Beam

The radiation emitted from the oscillating electrons is directed along the 20 meter optical cavity that is enclosed with a mirror at each end. One mirror merely reflects the optical beam into the cavity. The mirror at the other end is approximately 50% transparent to infrared radiation. A portion of the laser passes through the partially reflective mirror and is sent to the beam director before it leaves the ship to hit a target.

The emitted radiation is reflected along the optical cavity collinear with the electron beam, thus stimulating the electrons to emit coherent energy to increase the power of the optical beam. The phase and relative positions of the electron and optical beams is critical to achieving high powers. The electron and optical beam pulses must overlap through the undulator to exchange energy. Both the distance between the optical mirrors and the alignment of the mirrors and the undulator are critical to laser operation (Fiorani 4-7).

B. VIBRATION ENVIRONMENT FOR A SHIPBOARD FREE ELECTRON LASER

The vibration environment on a ship is quite harsh. The ship is constantly moving at low frequencies due to maneuvering and the seas. Running equipment creates both acoustic noise and vibration through the structure. The vibration environment on a naval ship will be discussed in generic terms, not specific to any platform, since the platform on which an FEL will be used is still unknown.

The motion of a ship is characterized by low frequency large amplitude oscillations. A ship's roll, pitch and yaw depend on the physical characteristics of the ship such as mass and size, the sea state, and the speed of the ship. Table 1 below lists maximum allowable motion for the FFG-7 class of frigates. The "Withstand" conditions are the most extreme motion a FFG-7 class ship should experience. Fortunately, the entire platform of the FEL moves with the ship. This motion does not present a big alignment issue for the most critical components of the laser if the components are mounted rigidly to the ship. Alignment could be a problem due to ship's motion if extensive passive isolation is used to mount the FEL components. The motion of the ship does present a targeting challenge to direct the laser beam accurately at a target.

	Normal Operating Conditions		Reduced Operating Conditions		Withstand Conditions	
Sinusoidal	Amplitude (deg.)	Minimum Period (sec)	Amplitude (deg.)	Period (sec)	Amplitude (deg.)	Period (sec)
Roll	± 25	8.5	± 35	8.5	± 45	8.5
Pitch	± 5	7	± 8	7	± 15	7
Yaw	± 2.5	7	± 4	7	± 7.5	7

Table 1. FFG-7 Maximum Amplitude, Minimum Period Motions. From [Allen 28]

The most critical vibration on a ship for precise jitter control is low frequency broadband disturbance. MILSTD-167-1A establishes testing requirements for placing equipment on a ship. A new piece of equipment must be tested by vibrating the equipment at a prescribed amplitude and frequency for each axis (x, y, z) for a certain

period of time for an exploratory test, variable frequency test, and endurance test. The exploratory test is conducted to discover any critical resonance frequencies by sweeping the frequency at integral values from 4 to 33 Hz in 15 second time intervals at a single amplitude of 0.01 inches. The variable frequency test requires a five minute hold at each integral frequency at the amplitudes and frequencies prescribed below in Table 2. These resonance tests are followed by a longer endurance test at each of the identified resonant frequencies, and can be up to 2 hours duration. This procedure is carried out to prevent equipment failure or malfunction at sea, which cannot be assured if the test fails or is waived.

Frequency Range (Hz)	Vibration Table Single Amplitude (inch)
4 to 15	0.030 ±0.006
16 to 25	0.020 ±0.004
26 to 33	0.010 ±0.002

Table 2. MIL-STD-167-1A Variable Frequency Test Requirements.

This series of vibration tests is clearly a worst case operating environment to test the equipment. It is unlikely that an actual piece of equipment on an underway ship would experience these amplitudes of vibration from all three axes at the same time. The Habitability section of ANSI S2.25-2004 states that the actual vibration allowed on a ship is half of that tested for in the MIL-STD-167-1A tests. Therefore, the worst case vibration will be considered half of the amplitude of the MIL-STD-167-1A test shown in Table 2.

It is noted that this description of the vibration environment is somewhat ambiguous concerning its effect on operation of the FEL. Only the relative motion of the critical components of the FEL needs to be considered. There is no impact on FEL operation if the optical mirrors, the undulator, and the electron beam are disturbed at the same amplitude, frequency and phase. A modal analysis of the area of the ship that the FEL will be mounted would provide critical vibration information such as critical vibration modes of the floor that would contribute to both translational and rotational

disturbances. Additionally, an acoustic survey of the intended area of installation would provide additional data, although acoustic noise on a ship is less significant than structural vibration.

C. VIBRATION LIMITS FOR A FREE ELECTRON LASER

An FEL needs to be vibration isolated sufficiently to function properly on a ship. Since the weapon is still in the design stage, the tolerable limits for vibration are not known with certainty. The limits for vibration displacement have been estimated three ways. First, the limits for linear and angular displacement for certain key components of the FEL have been estimated using computer modeling. Second, the limits for linear displacement have been estimated by measuring the vibration of a functioning FEL. Third, limits of vibration are established by measuring the vibration of a standard laboratory environment.

1. Postulated Limits from Computer Modeling

The position of the bending magnets has a tolerance of about one millimeter to control the electron beam. The critical tolerance is at the center of the undulator where the electron beam and optical beam need to be less than about ten microns. This corresponds to about a one microradian tolerance for mirror tilt (Colson).

2. Measured Vibration on a Functioning Free Electron Laser and in a Laboratory

Several Free Electron Lasers have proven to work successfully with little active or passive vibration control in a laboratory environment. Therefore, if the vibration environment of a laboratory can be replicated on a ship, the Free Electron Laser would function properly. Vibration measurements were made on an FEL and in a laboratory as described below.

a. Test Equipment for Measurement of Vibration

(1) Triaxial Linear Accelerometer. One triaxial linear accelerometer was used to take all acceleration measurements. It is a PCB Model 354B33 pieozelectric accelerometer, Serial Number 454. It has a frequency response of ±5% from 1 to 2000 Hz. The accelerometer has three quartz sensing elements configured for shear displacement with a built-in charge amplifier. A 10-32 thru bolt was attached through the titanium housing to a magnetic mounting base for mounting the accelerometer in all applications. A nominally 4 mA constant external current source is required for operation, which was supplied by the Stanford Signal Analyzer. A calibration certificate for each axis of the accelerometer is provided in Appendix A (PCB Piezotronics Inc.).

(2) Stanford Signal Analyzer. A Stanford Research Systems Model SR785 2 Channel Dynamic Signal Analyzer was used to process and record the voltage measured from the output of the accelerometer. Although the analyzer has two signal inputs, only one signal, or axis, was measured at a time from the accelerometer. The analyzer was configured for a Fast Fourier Transform (FFT) measurement group over a frequency span from 0 to 400 Hz with a sampling rate of 262 kHz and FFT resolution of 800 lines. The SR785 passes the input signal through an analog anti-aliasing filter to remove all frequency components above 102.4 kHz before gathering the time records and transforming them into spectra (Stanford Research Systems 2-7). The input was configured for ICP coupling, which provides a 4.8 mA current source to the transducer (Stanford Research Systems xii). The time record was windowed with a Blackman-Harris window. Sixteen root mean square (rms) averages were performed. The log of the magnitude of the signal in power spectral density level (psdl) units of dB Vpk/√Hz over a linear frequency range in units of Hertz was recorded on a 3 ½" disk and transferred to a computer for further processing.

b. Accelerometer Mounting Locations

The triaxial accelerometer was mounted magnetically in several locations for vibration measurements. The first set of measurements was taken at an actual FEL in

the FEL tunnel at Stanford University, which is in the basement of the W.W. Hansen Experimental Physicals Laboratory. The second set of measurements was taken in the basement of Spanagel Hall in Room #042 at the Naval Postgraduate School (NPS). The z-axis is in the vertical direction when the accelerometer is mounted horizontally, which it was for all measurements. The x-axis and y-axis configuration is described below for each measurement.

(1) Wiggler of FEL. The accelerometer was mounted on top of the wiggler of the FEL magnetically with the x-axis placed in the direction of the beam of the laser. The y-axis measured acceleration perpendicular and horizontal to the beam.

(2) Base of FEL. The accelerometer was mounted on top of the base to the FEL magnetically in the vicinity of the wiggler, with the same orientation as when it was mounted on the wiggler as discussed above.

(3) Spanagel Hall Room #042. The accelerometer was mounted magnetically on the doorway in Spanagel Hall Room #042. Again, the z-axis was oriented vertically, with the x-axis and y-axis parallel to the floor.

c. Results of Accelerometer Measurements

The first set of vibration measurements was conducted on March 9, 2007 at Stanford University's FEL. The Second set of measurements was taken with the same equipment on April 18, 2007 at NPS.

(1) Data Organization by Filename. The measured data from each run were saved as an ASCII file on a 3 ½" disk. The data were then transferred to a computer at the Naval Postgraduate School, in a .txt format. The first data point, at 0 Hz, was deleted from each file, to avoid divide-by-zero errors in later calculations. The files were renamed for convenience, using the nomenclature described below. The first letter distinguishes which axis of the accelerometer was measured, either "x", "y" or "z". The next word describes the location of the measurement, either "wiggler", "floor", or "Spanagel". The last number describes which data run if more than one were taken at the

same location for a given axis. The files were inputted into MATLAB using the *inputdata* function, as shown in Appendix B.

(2) Processing Measurements from Linear Accelerometer. The recorded vibration data is a power spectral density level (psdl) with units of dB $V_{pk}/\sqrt{Hz}$ over a linear frequency range in units of Hertz. The psdl was converted to power spectral density (psd) with units of V_{rms}^2/Hz by

$$psd = \frac{1}{2} 10^{\frac{psdl}{10}} \tag{2.1}$$

where the factor one half converts from peak to rms values. This psd was then converted to units of $(m_{rms}/s^2)^2/Hz$ by dividing by the square of the given voltage sensitivity for each axis of the accelerometer and multiplying by the square of the constant g (g=9.81 m/s^2). This psd was integrated twice by dividing by ω^4 to obtain the displacement power spectral density in units of m_{rms}^2/Hz, where $\omega=2\pi f$ and f is the frequency in Hertz.

The area under this power spectral density function between any upper and lower frequency limits gives the mean square value of the data (Bendat and Piersol 52).

$$\psi_x^2(f_1, f_2) = \int_{f_1}^{f_2} G_{xx}(f) df \tag{2.2}$$

This integral was performed by summing the products of the bin widths (800 line FFT resolution/400 Hz range=0.5 Hz) and the displacement power spectral densities for a desired frequency range. The square root of this mean square value gives the root mean square value in units of m_{rms} for a given frequency range.

(3) Vibration Measurement Results. The total displacement from 1-400 Hz disturbances for each axis at each location is shown below in Figure 3.

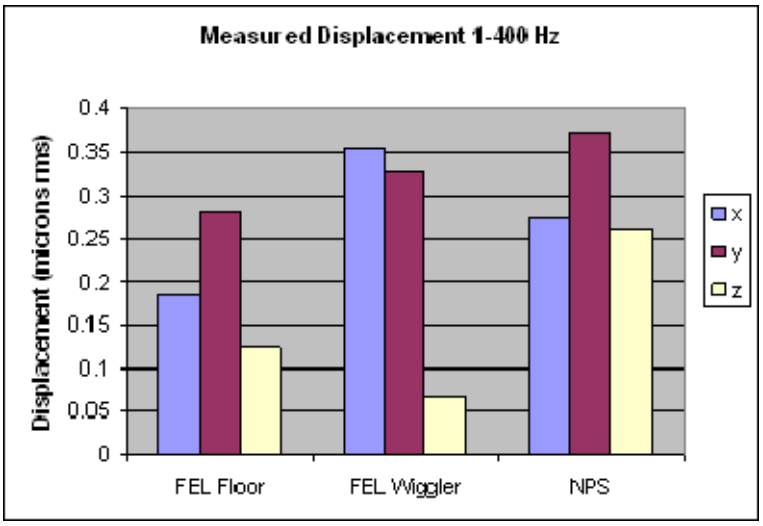

Figure 3 Displacement Measured from Accelerometer

3. Discussion of Vibration Limits

Computer simulations have shown that the control of the optical beam has the most limiting vibration requirement at 1 μrad. Displacement of less than a half of micron over the length of Stanford's FEL without any active vibration isolation yields clearly much less jitter than the estimated limit of 1 μrad. The vibration measurements of an actual FEL were made as a reality check to compare to the postulated computer simulation limits. As expected, the vibration of Stanford's FEL is not affected by vibration much less than the predicted limits from computer simulations. If vibration levels such as these can be achieved for a shipboard FEL, then the risk of failure due to vibration is very small.

THIS PAGE INTENTIONALLY LEFT BLANK

III. REVIEW OF VIBRATION CONTROL THEORY

A. PASSIVE VIBRATION ISOLATION

1. Single Stage Isolation

The classic single-stage vibration isolation system is modeled as a linear, one-dimensional mass-spring-dashpot system mounted on a harmonically exited base, as shown in Figure 4 below. The spring, *k*, and the dashpot, *c*, represent the parallel combination of springs and dashpots supporting the mass, *m*. The mass may represent, for example, a component of an FEL. The support, *s*, is harmonically excited at a peak displacement amplitude of x_s. The resulting peak displacement of the harmonic oscillation of the mass is given the symbol x_m. The motional transmissibility, which is the displacement of the mass divided by that of the support, can be found by solving the equivalent electrical circuit, which is shown in Figure 4 below.

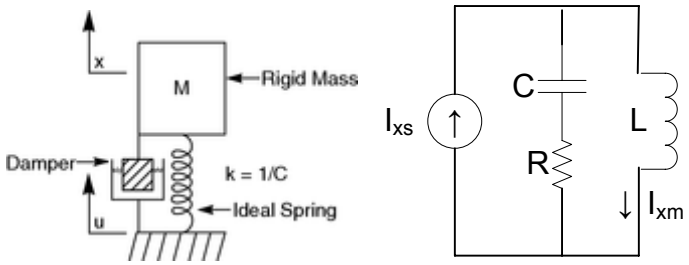

Figure 4 Passive Vibration Mounting. After [Newport]

The current in each branch represents vertical velocity. The support isolation is assumed given, and so is modeled as a current source. The mass is represented by an inductor, *L*. The spring is modeled as a capacitor, *C*, where *C=1/k*. The dashpot is modeled as a resistor, *R*, which is equal to *c*. The transmissibility is found by dividing the current from the source, I_{xs} by the current through the inductor, I_{xm}. This relationship is found by using Kirchoff's current law:

$$T = \frac{I_{xs}}{I_{xm}} = \frac{R + \frac{1}{j\omega C}}{R + \frac{1}{j\omega C} + j\omega L} \tag{3.1}$$

This can be simplified by taking the absolute value of both sides and substituting

$$r = \frac{f}{f_n} \tag{3.2}$$

$$f_n = \frac{1}{2\pi}\sqrt{\frac{1}{LC}} \tag{3.3}$$

$$\zeta = \frac{R}{2R_{char}} \tag{3.4}$$

$$R_{char} = \sqrt{\frac{L}{C}} \tag{3.5}$$

Where r is the frequency ratio, f_n is the natural frequency, ζ is the damping ratio, and R_{char} is the characteristic resistance which is equal to half of the critical damping coefficient.

The final result for transmissibility for this equivalent circuit of single stage isolation is

$$T = \sqrt{\frac{1 + (2\zeta r)^2}{(1 - r^2)^2 + (2\zeta r)^2}} \quad \text{(Beranek and Ver 558)} \tag{3.6}$$

The transmissibility plotted versus r for a variety of damping ratios is shown below in Figure 5. Support motion, x_s, near the resonance peak is actually amplified, depending on the damping factor. This system is designed to be used when the expected excitation frequencies are well above the resonance of the system, or in the isolation range. Increased damping reduces the response at resonance, but increases the transmissibility in the isolation range.

The above model assumed viscous damping, which is a resistive force proportional to velocity. Viscous damping problems such as this one can generally be

solved analytically. Damping that occurs in practical isolators is better modeled as structural damping, which produces a retarding force proportional to displacement. The transmissibility for a structurally damped system is given by

$$T = \sqrt{\frac{1+(\eta)^2}{(1-r^2)^2+(\eta)^2}} \quad \text{(Beranek and Ver 561)} \qquad (3.7)$$

where η is the loss factor of the system. Viscous and structural damping can be compared for the same amplification at the natural frequency when $\eta = 2\zeta$ as shown in Figure 5. Structural damping actually produces lower transmissibility in the isolation range than viscous damping for $\eta = 2\zeta$.

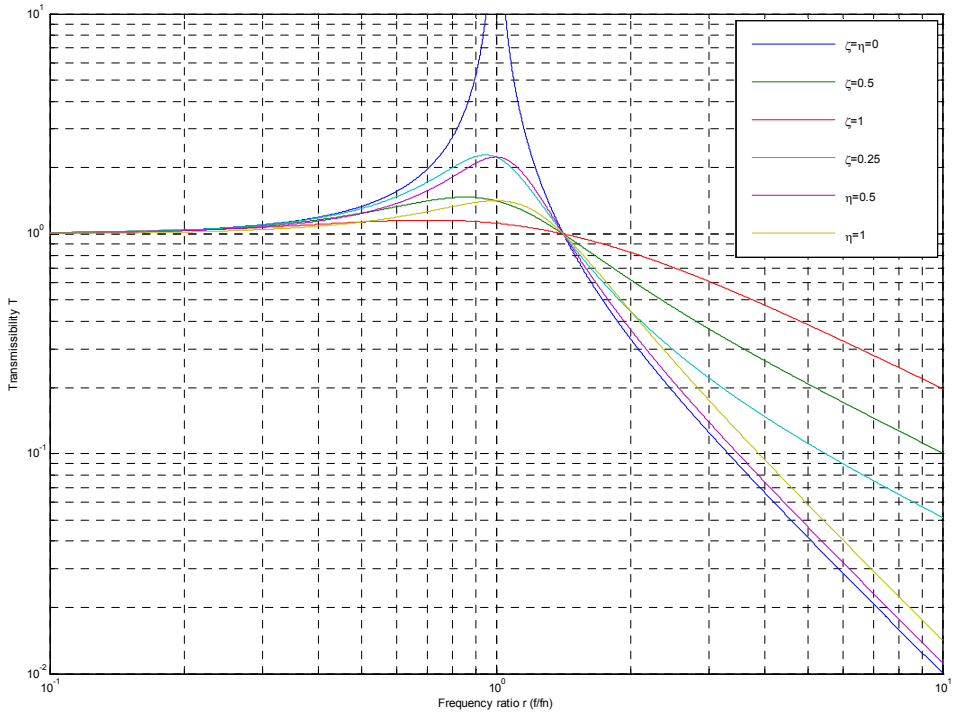

Figure 5 Transmissibility of a Simple Mass-Spring-Damper System. After [Beranek and Ver 560]

2. Two Stage Isolation

An additional stage of passive isolation can be added by using an isolator with some mass to reduce the transmissibility at higher frequencies. The force of the vibration is reduced by the inertia force of the mass, m_i, before being transmitted. This set-up is shown below in the simple two stage isolation diagram of Figure 6. The isolations, k_1 and k_2, are only springs with no damping.

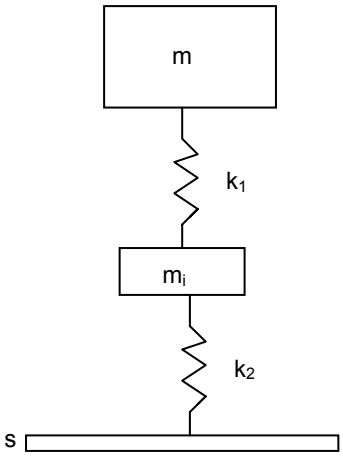

Figure 6 Two-Stage Isolation

The two-stage isolator transmissibility is shown below in Figure 7, Figure 7 compared to single-stage isolation. Both of the spring constants are unity for convenience and the ratio of the intermediate mass frequency to the natural frequency of the mass is five. If damping were included in the isolations, the two resonant peaks would be lower. This plot shows how much faster the transmissibility drops off above the second resonance for two stage isolation. Two-stage isolation is much more effective against high frequency disturbances, but it still amplifies low frequency vibration. If incorporated in the design phase, in many cases the intermediate mass does not need to be dead extra weight. For example, some necessary structural components of the FEL could act as intermediate masses without increasing the overall mass of the plant.

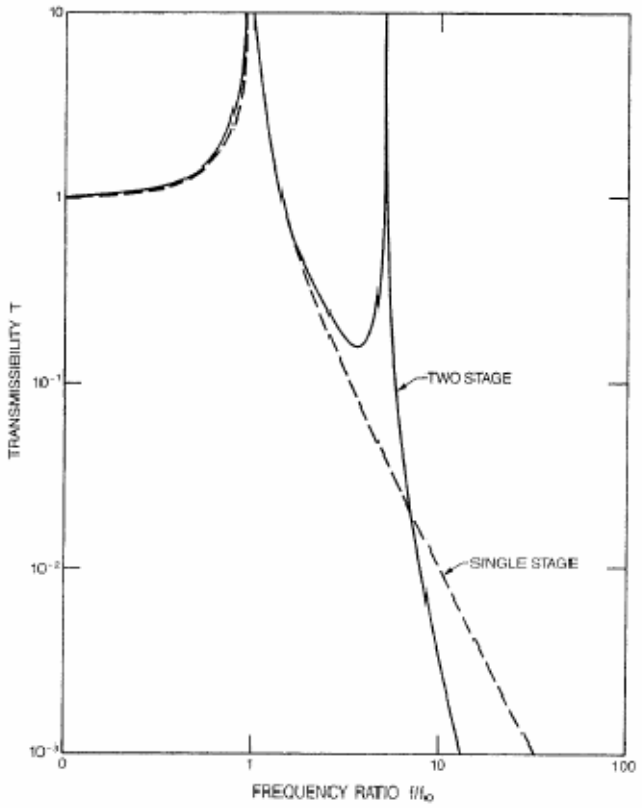

Figure 7 Transmissibility of Two-Stage System. From [Beranek and Ver 574]

B. ACTIVE VIBRATION ISOLATION

Active vibration isolation employs some kind of motion or error sensor, an electronic controller, and an actuator, to control unwanted vibration. Two major types of controllers that can be used for active vibration control are feedback and feedforward. The reader is referred to Kuo for a more detailed explanation of terms. The feedback method can be used with either fixed gains or with adaptively changing gains. A feedback controller is very useful for addressing an unknown or immeasurable disturbance, when no disturbance reference signal is available. Feedforward can be much more effective if a reference signal of the disturbance is available, especially when used in an adaptive controller.

1. Fixed Feedback

A fixed feedback controller can be designed using a pole-placement method, the root-locus method, or with a quadratic optimal regulator. The reader is referred to Ogata for a background on fixed feedback controllers. A Linear Quadratic Gaussian regulator (LQG), a type of quadratic optimal regulator, was designed and used to test a linear time invariant (LTI) controller for various types of disturbances. The pole-placement method can lead to a trial and error approach to designing feedback gains, but the LQG can be used to determine optimal gains in a systematic approach.

a. Linear Quadratic Regulators

A Linear Quadratic Regulator (LQR) requires a good mathematical model of the open-loop system to calculate the optimal gains to use for full state feedback. Any immeasurable states must be estimated using an observer or Kalman estimator. A Linear Quadratic Guassian (LQG) regulator is an LQR controller with a Kalman estimator. The open-loop system can be identified using a number of methods as discussed in Chapter V. Every system has a set number of state variables, which are not unique, to completely specify the dynamical state of the system, which system is linear for an LQR. The system is placed in the state-space model time-invariant form given by

$$\dot{\mathbf{x}} = \mathbf{A}\mathbf{x} + \mathbf{B}\mathbf{u} \tag{3.8}$$

$$\mathbf{y} = \mathbf{C}\mathbf{x} + \mathbf{D}\mathbf{u} \tag{3.9}$$

where $\mathbf{x}$ is the state vector, $\mathbf{u}$ is the input vector and $\mathbf{y}$ is the output vector. The matrix $\mathbf{A}$ is the state matrix, $\mathbf{B}$ is input matrix, $\mathbf{C}$ is the output matrix, and $\mathbf{D}$ is the direct transmission or feed through matrix, which is typically zero.

The controller regulates the output through full state feedback by using the input

$$\mathbf{u} = -\mathbf{K}\mathbf{x} \tag{3.10}$$

The optimal gains, $\mathbf{K}$, are chosen to minimize the quadratic cost index

$$J = \int_0^\infty (\mathbf{x}^T \mathbf{Q} \mathbf{x} + \mathbf{u}^T \mathbf{R} \mathbf{u}) dt \tag{3.11}$$

The weighting matrices, $\mathbf{Q}$ and $\mathbf{R}$, are chosen to balance the amount of control used and the allowable error. For a given set of weighting matrices, the LQR will determine an optimal gain vector. MATLAB was used to solve for these optimal gains using the *lqr* function.

The state space model is applied in discrete time form on the actual test bed. The MATLAB command *lqrd* was used to solve for the optimal gains in discrete time. The state space model in discrete time with step k is of the form

$$\mathbf{x}(k+1) = \mathbf{A}\mathbf{x}(k) + \mathbf{B}\mathbf{u}(k) \tag{3.12}$$

$$\mathbf{y}(k) = \mathbf{C}\mathbf{x}(k) + \mathbf{D}\mathbf{u}(k) \tag{3.13}$$

where the system matrices $\mathbf{A}$, $\mathbf{B}$, $\mathbf{C}$ and $\mathbf{D}$ are different than those for continuous time. The full state feedback controller with $\mathbf{D}$ is shown below in Figure 8 .

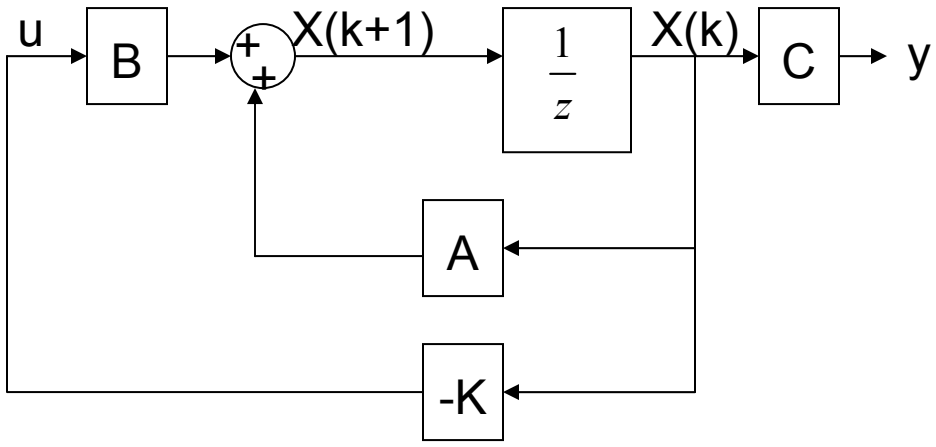

Figure 8 Full State Feedback Controller in Discrete Time

An LQR as discussed above will have poor tracking performance if the system has no integrator. An integrator must be added to the feedback controller to track a target reference, r, since the system on the Laser Jitter Control (LJC) table is a type zero

system. The target reference is the desired output of the system. This requires adding an additional state variable, ξ, to the open-loop system determined during system identification that is defined by

$$\xi(k+1) = r - y(k) = r - \mathbf{C}\mathbf{x}(k) \tag{3.14}$$

The *lqr* MATLAB command will solve for the optimal gains for the state feedback and the integral gain k_I. The resulting LTI controller with an integrator is shown below in Figure 9.

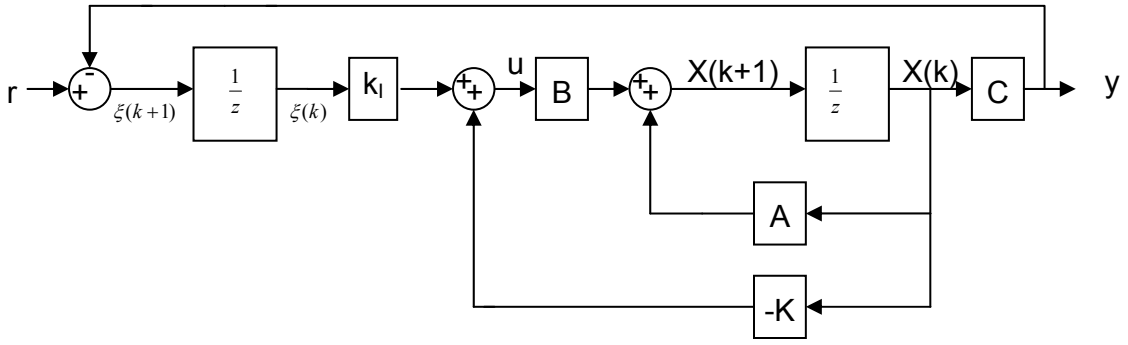

Figure 9 Full State Feedback Controller with an Integrator

2. Adaptive Feedback

An adaptive feedback controller responds to changes in disturbances that require a change of gains, which may no longer be optimal. Some type of adaptive filter is usually employed to minimize the mean-square error (MSE) of the output. Adaptive feedback does not require a reference signal of the disturbance. A typical broadband feedback acoustic noise control (ANC) system is shown below in Figure 10. Acoustic noise control is shown here as an example of active control. The same techniques can be applied to active vibration control. When a reference signal is available, an adaptive feedforward controller will perform better. No experiments using adaptive feedback were performed on the LJC Testbed.

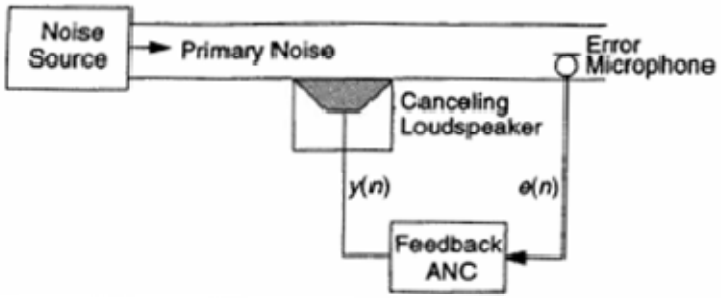

Figure 10 Single-channel Feedback ANC System. From [Kuo 12]

3. Adaptive Feedforward

An adaptive feedforward controller senses a disturbance using a reference signal and drives the controller to minimize the error signal. A typical broadband feedforward application in ANC is shown below in Figure 11.

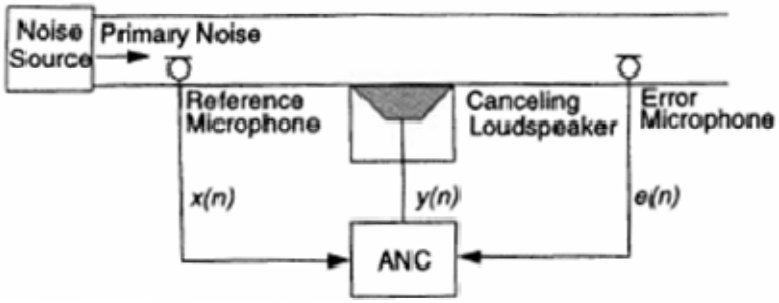

Figure 11 Single-channel Broadband Feedforward ANC System in a Duct. From [Kuo 10]

An adaptive feedforward controller setup must have a highly coherent and causal reference signal. The reference signal must be highly correlated to the actual disturbance to reduce the noise at the error signal. A causal reference signal senses a disturbance early enough for the controller to compensate for the disturbance before it reaches the error sensor. This depends on the speed of the disturbance and the speed of the controller. The controller can reduce the undesired noise at the error sensor even if the reference signal isn't causal if the disturbance is slowly changing compared to the frequency response of the controller. This is the case for the LJC Testbed since the system samples at 2000 Hz for disturbances of concern below 40 Hz.

The adaptive feedforward acoustic noise control system shown in Figure 11 is described in more detail below by a block diagram in Figure 12. The ANC system is complicated by secondary-path effects. The secondary-path transfer function *S(z)=R(z)S'(z)* takes into account the secondary transfer function *S'(z)* from the output *y(n)* to the summing junction, which is the open-loop system response, and the residual transfer function *R(z)* from the summing junction to the error sensor *e(n)*. The primary transfer function *P(z)=R(z)P'(z)* takes into account *P'(z)* from the reference sensor *x(n)* to the summing junction, and the residual transfer function *R(z)* (Kuo 59).

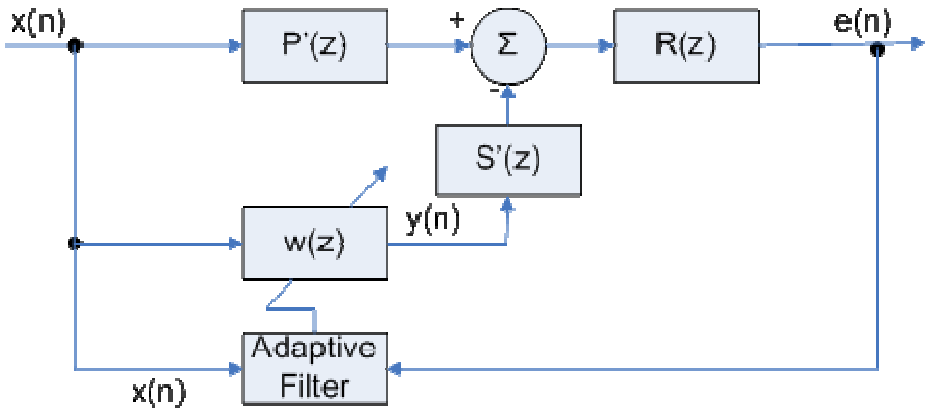

Figure 12 Block Diagram of an ANC system. After [Kuo 59]

Many different reference signals may be available. Accelerometers can be good references, but are not effective at low frequencies. An optical reference can be highly coherent even at low frequencies, since it can measure actual displacement due to the disturbance instead of acceleration like an accelerometer. An optical reference can measure disturbances accurately between two objects that are moving relative to each other. An accelerometer measures in reference to an inertial reference frame, which information may be undesirable on a moving platform such as a ship.

An adaptive filter is merely a digital filter with an adapting algorithm to adjust the filter's coefficients as required. The adaptive filter's algorithm is usually designed to minimize the mean-square error (MSE), or the expected value of the squared error. The adaptive filters used on the LJC Testbed are transversal filters, as shown below in Figure

13. Two major types of adaptive filters will be discussed and tested for disturbance rejection: Least Mean Square (LMS) and Recursive Least Square (RLS) algorithms.

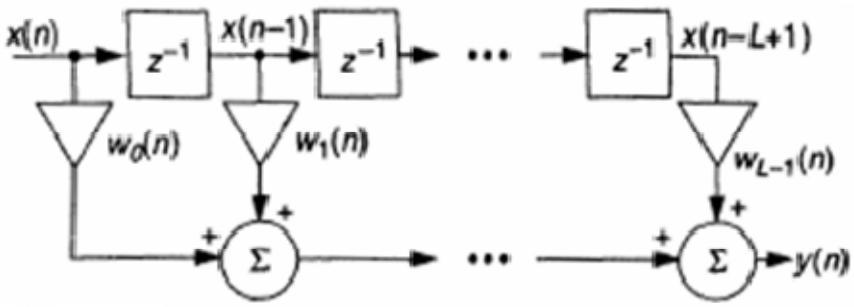

Figure 13 Transversal Filter. From [Kuo 18]

a. The Least Mean Square Algorithm

The LMS algorithm is one of the most simple adaptive algorithms used in disturbance rejection and is considered somewhat of a standard. The following explanation and derivation of the LMS algorithm follows Kuo, but will be explained in the context of an adaptive feedforward controller (Kuo 19-26). The reference signal history is stored in a column matrix under the matrix $\mathbf{x}(n)$ for each discrete time sample up to the maximum number of stages L. A weighting vector $\mathbf{w}(n)$ is defined as a row of weighting coefficients for each stage of the filter at time n. The filter determines its output signal $y(n)$ and error signal $e(n)$ as follows:

$$y(n) = \mathbf{w}^T(n)\mathbf{x}(n) \tag{3.15}$$

$$e(n) = d(n) - s(n) * y(n) \tag{3.16}$$

The value *d(n)* is the desired response, which is zero in the adaptive feedforward setup. The output of the adaptive filter *y(n)* is linearly convoluted with the secondary impulse response, *s(n)*, of the plant.

The LMS algorithm uses the method of steepest descent, which is a gradient-based algorithm, to determine the optimal weighting coefficients. The steepest descent method is an iterative technique that takes steps, size μ, in the direction of the negative of the gradient of the surface of the MSE show in Figure 14 below as follows:

$$\mathbf{w}(n+1) = \mathbf{w}(n) - \frac{\mu}{2}\nabla\xi(n) \tag{3.17}$$

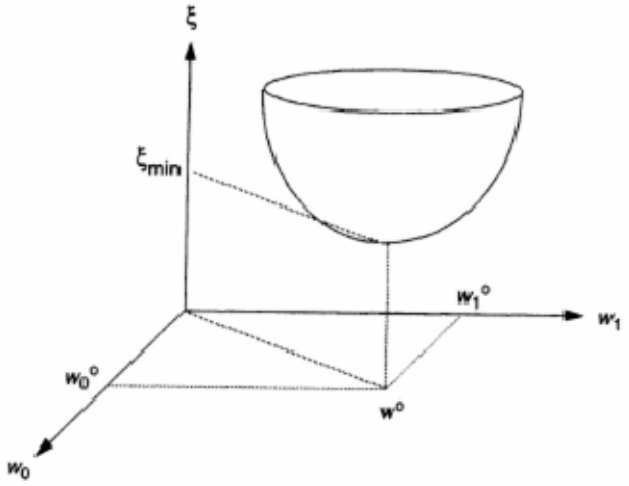

Figure 14 MSE Surface. From[Kuo 21]

The gradient of the MSE is approximated as follows for the LMS algorithm:

$$\nabla\hat{\xi}(n) = \nabla e^2(n) = 2[\nabla e(n)]e(n) = 2[-\mathbf{x}(n)]e(n) \tag{3.18}$$

This gradient estimated is substituted into 3.18 above to yield the computationally efficient stochastic gradient algorithm (Kuo 23-25)

$$\mathbf{w}(n+1) = \mathbf{w}(n) + \mu\mathbf{x}(n)e(n) \tag{3.19}$$

The control signal output of the adaptive filter *y(n)* goes through the plant designated as the secondary transfer function *S(z)*. This mismatch in time between the error signal and the reference signal can cause convergence problems. One common solution to this problem is to filter the reference signal with an estimate of the secondary transfer function, which is known as the Filtered-X Least Mean Square (FXLMS)

algorithm, as shown below in Figure 15. An accurate mathematical model of the system is needed to filter the reference to ensure convergence.

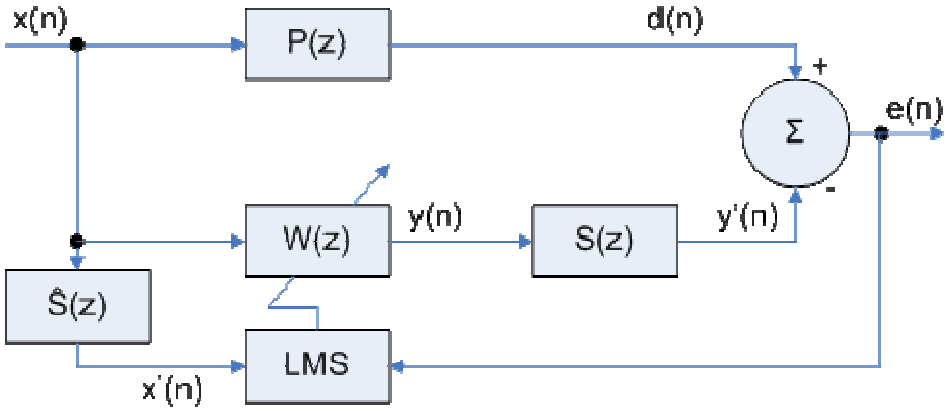

Figure 15 FXLMS Diagram. From [Kuo 64]

b. Recursive Least Square Algorithm

The Recursive Least Square (RLS) algorithm converges faster and yields smaller errors than an LMS filter. The RLS method updates the weighting vector at each time step by computing the change in the weighting vector necessary to minimize the cost function. The major difference compared to the LMS method is that the RLS algorithm's cost function has a memory of errors with a forgetting factor $0 \leq \lambda < 1$. The LMS method minimizes the cost function which is only based on the current error. The derivation of the RLS algorithm follows Kuo (257-263). The cost function is redefined as

$$\xi(n) = \sum_{i=1}^{n} \lambda^{n-1} e^2(i) \tag{3.20}$$

The error signal at time *i* is defined as

$$e(i) = d(i) - \mathbf{w}^T(n)\mathbf{x}(i) \tag{3.21}$$

where the input and weighting vectors are defined the same as for the LMS derivation above. Again, the desired signal, *d(i)* is zero for an adaptive feedforward application.

The optimum weight vector can be found by differentiating the expanded cost function with respect to $\mathbf{w}(n)$ and setting to zero. This yields the optimum weight vector

$$\mathbf{w}^o(n) = \mathbf{p}(n)\mathbf{R}^{-1}(n) \tag{3.22}$$

The sample crosscorrelation vector is defined as

$$\mathbf{p}(n) = \sum_{i=1}^{n} \lambda^{n-i} d(i)\mathbf{x}(i) \tag{3.23}$$

The sample autocorrelation matrix is defined as

$$\mathbf{R}(n) = \sum_{i=1}^{n} \lambda^{n-i} \mathbf{x}(i)\mathbf{x}^T(i) \tag{3.24}$$

Unfortunately, calculating the inverse of the sample autocorrelation matrix can be a computationally large operation if there are a large number of stages in the filter. Instead, $\mathbf{R}(n)$ can be found recursively to simplify the calculation by expanding xx above as follows:

$$\begin{aligned} \mathbf{R}(n) &= \sum_{i=1}^{n-1} \lambda^{n-i} \mathbf{x}(i)\mathbf{x}^T(i) + \lambda^0 \mathbf{x}(n)\mathbf{x}^T(n) \\ &= \lambda \mathbf{R}(n-1) + \mathbf{x}(n)\mathbf{x}^T(n) \end{aligned} \tag{3.25}$$

This eases the computational burden somewhat, but the inverse $\mathbf{R}^{-1}(n)$ is still required to find the optimum weighting vector. The inverse can be approximated recursively from the previous $\mathbf{R}^{-1}(n-1)$ according to the following matrix inversion lemma (Kuo 259):

$$(\mathbf{A} + \mathbf{BCD})^{-1} = \mathbf{A}^{-1} - \mathbf{A}^{-1}\mathbf{B}(\mathbf{DA}^{-1}\mathbf{B} + \mathbf{C}^{-1})^{-1}\mathbf{DA}^{-1} \tag{3.26}$$

where

$$\mathbf{A} \equiv \lambda \mathbf{R}(n-1) \tag{3.27}$$

$$\mathbf{B} \equiv \mathbf{x}(n) \tag{3.28}$$

$$\mathbf{C} \equiv 1 \tag{3.29}$$

$$\mathbf{D} \equiv \mathbf{x}^T(n) \tag{3.30}$$

This yields the following inverse matrix that is calculated recursively:

$$\mathbf{R}^{-1}(n) = \lambda^{-1}\mathbf{R}^{-1}(n-1) - \frac{\lambda^{-1}\mathbf{R}^{-1}(n-1)\mathbf{x}(n)\mathbf{x}^T(n)\lambda^{-1}\mathbf{R}^{-1}(n-1)}{\mathbf{x}^T(n)\lambda^{-1}\mathbf{R}^{-1}(n-1)\mathbf{x}(n)+1} \tag{3.31}$$

The inverse of the sample autocorrelation matrix is redefined for clarity as

$$\mathbf{Q}(n) = \mathbf{R}^{-1}(n) \tag{3.32}$$

Additionally, the Kalman gain vector is defined as

$$\mathbf{k}(n) = \frac{\lambda^{-1}\mathbf{Q}(n-1)\mathbf{x}(n)}{\lambda^{-1}\mathbf{x}^T(n)\mathbf{Q}(n-1)\mathbf{x}(n)+1} \tag{3.33}$$

to simplify the recursion relationship 3.32 above as

$$\mathbf{Q}(n) = \lambda^{-1}\mathbf{Q}(n-1) - \lambda^{-1}\mathbf{k}(n)\mathbf{x}^T(n)\mathbf{Q}(n-1) \tag{3.34}$$

From 3.22 above, the optimum weight vector can now be shown to be

$$\mathbf{w}(n+1) = \mathbf{w}(n) + \mathbf{k}(n)e(n) \tag{3.35}$$

where *e(n)* now includes the secondary plant impulse function and has been redefined as

$$e(n) = d(n) - s(n) * \mathbf{w}^T(n)\mathbf{x}(n) \tag{3.36}$$

to include only inputs from the current time.

One major disadvantage of an RLS filter is the number of multiplications required for each time sample, 2L2+4L, where L is the number of stages of the filter (Kuo 261). Therefore, the processing equipment may limit the number of stages that can be employed for a given sample time, or the hardware may even limit the sampling frequency. This could sacrifice performance if the optimum number of stages cannot be used.

For the same reasons discussed above in the LMS section, the Filtered-X Recursive Least Square (FXRLS) reference signal must be filtered with an estimate of the secondary plant to ensure convergence. A diagram of an FXRLS algorithm is shown below in Figure 16.

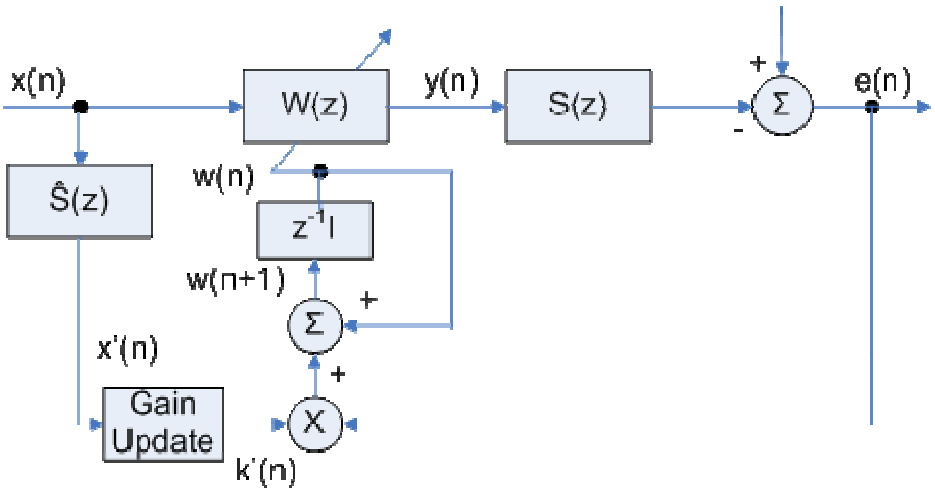

Figure 16 FXRLS Diagram. From [Kuo 264]

IV. EXPERIMENTAL SETUP

The Laser Jitter Control Testbed is an excellent platform to develop and test active control algorithms for jitter control that could be used on the Free Electron Laser. The experimental setup is designed to test active vibration control from three sources: a disturbance fast steering mirror (DFSM), an inertial shaker, and vibration from the floor. Multiple sources of vibration allow flexibility in testing both known and unknown disturbances for different applications of active vibration control.

A. LASER JITTER CONTROL TESTBED

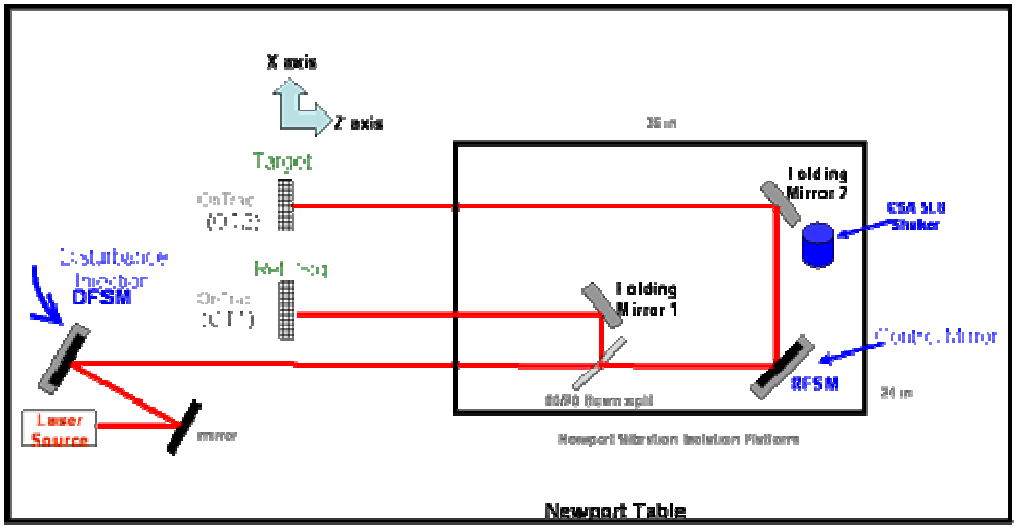

Figure 17 Laser Jitter Control Testbed

The Laser Jitter Control (LJC) Testbed is located in the Spacecraft Research and Design Center-Optical Relay Mirror Lab in Halligan Hall at the Naval Postgraduate School in Monterey, California. A Newport Optical Bench is floated on low pressure air to provide the base for optical components to reduce vibration from the building through the floor. The 2.5 mW 670 nm laser is split into multiple beams down the path to utilize laser position and disturbance information from three different detectors. The control fast steering mirror is mounted on an additional smaller Newport Vibration Isolation Platform, which is mounted on the optical bench to provide a means for an

inertial shaker to insert disturbance to some of the components. The main path of the laser goes from the source to the disturbance fast steering mirror, to the control fast steering mirror, and then to the detector OT2. The first position sensing detector, OT1, reads the laser position from a beam splitter after the DFSM. The other two detectors, OT2 and OT3, read the laser position after the laser is corrected at the controlling mirror, each providing references with different sources of disturbance: the detector OT3 is mounted on the smaller shaker platform while the detector OT2 is mounted on the main optical bench.

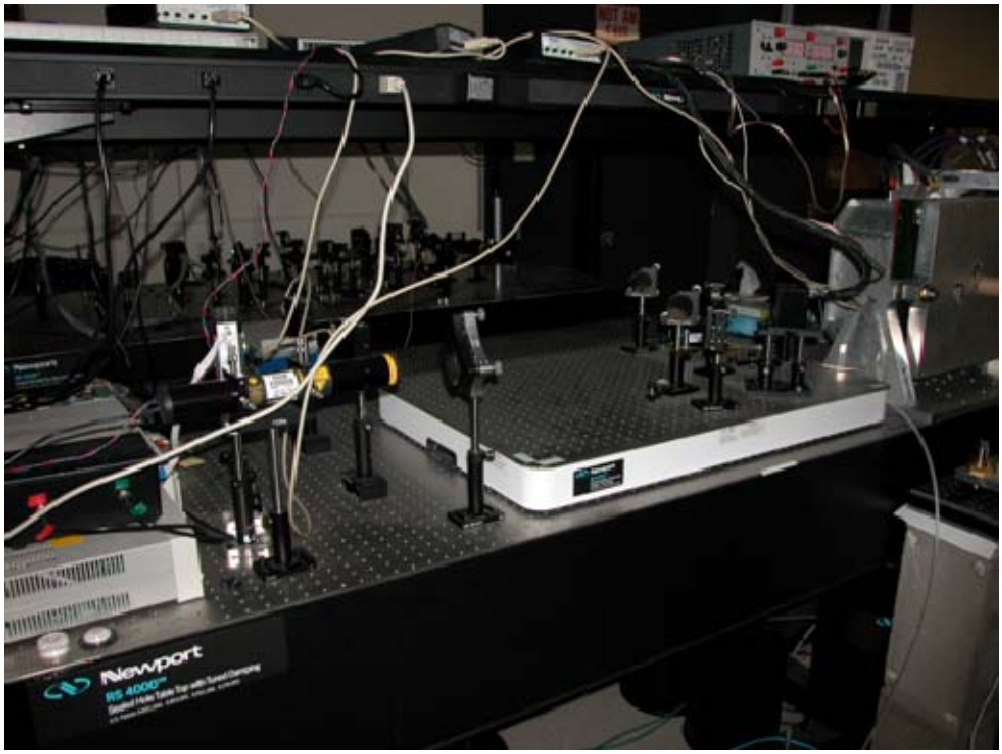

Figure 18 Laser Jitter Control Testbed

B. DETECTORS

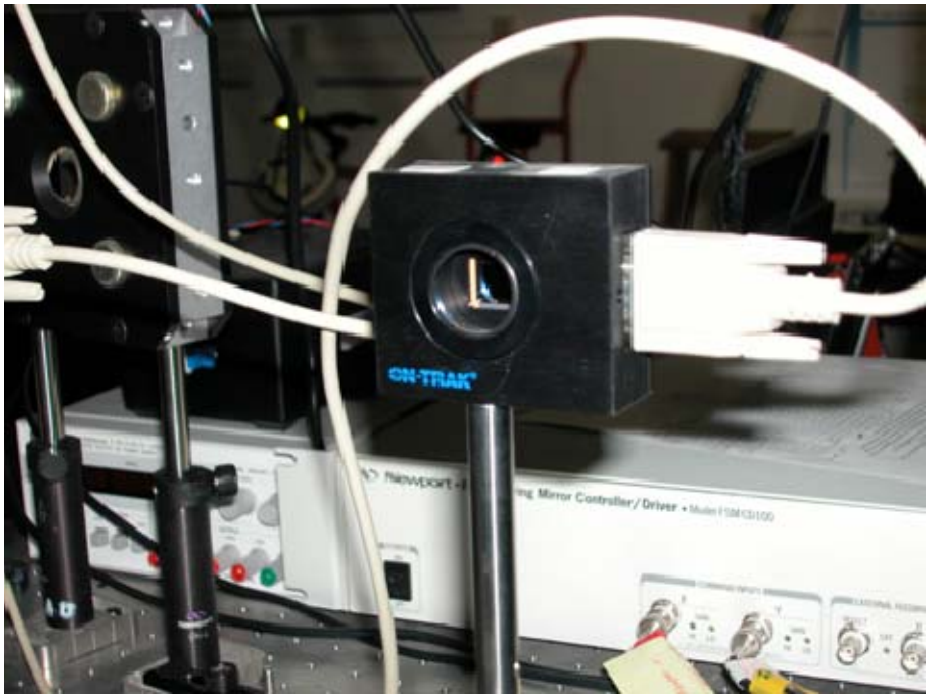

Figure 19 Position Sensing Module

Three ON-TRAK PSM2-10 Position Sensing Modules are used to measure the x and y positions of the laser at various points of the optical path. Combined with the ON-TRAK OT-301 Position Sensing Amplifiers, the detectors provide an analog voltage output of +/- 10 volts of the position of a laser beam. Each dualateral silicon module can detect light from 400-1100 nm at a typical resolution of 250 nm on a 10 mm by 10 mm screen. The amplifier has six gain settings that are set according to the input current ranges. OT1 and OT3 are set to a gain setting of two, while OT2 is set to a gain setting of one. The frequency response at both of these settings is reported by the manufacturer to be 16 kHz. The specifications and diagrams of the detector are shown in Appendix C.

C. FAST STEERING MIRRORS

1. Disturbance Mirror – Baker Fast Steering Mirror

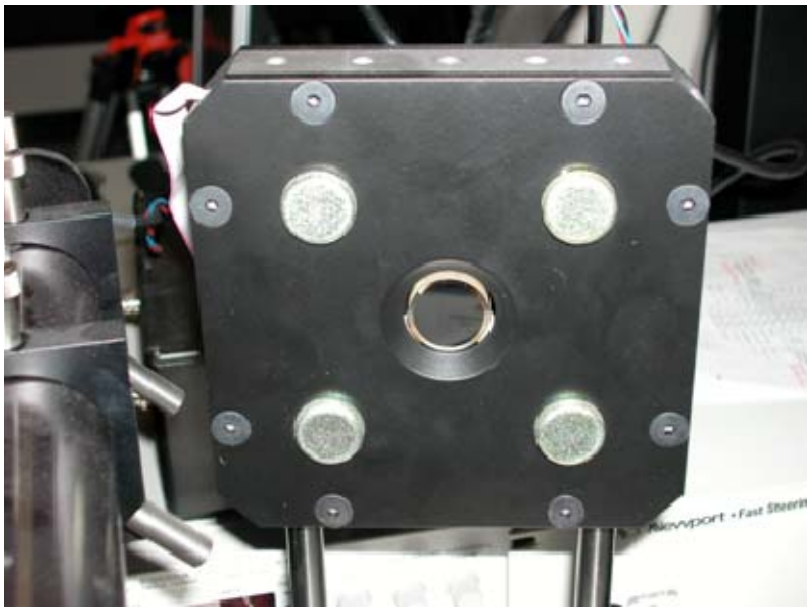

Figure 20 Baker Fast Steering Mirror

The disturbance fast steering mirror (DFSM) is a model "Light Force One" Baker fast steering mirror. A small one inch mirror suspended on springs is driven to provide a disturbance signal on the LJC Testbed. The noise equivalent angle is reported by the manufacturer to be less than 20 nanoradians. Unfortunately, the mirror does not output a position, and does not utilize closed loop controls. The coordinate system of the mirror is 45° relative to the table and to the coordinate system for the detectors. The mirror exhibited erratic behavior when controlled with a signal that crossed its own zero axis, as if it detected a large impulse. The Newport fast steering mirror did not exhibit this behavior. Due to this erratic behavior and the lack of position output, the Baker fast steering mirror was chosen as the disturbance mirror. A large bias was used to ensure that the control signal to the DFSM did not cross either the x or y axis. The mirrors specifications are included in Appendix C.

2. Control Mirror-Newport Fast Steering Mirror

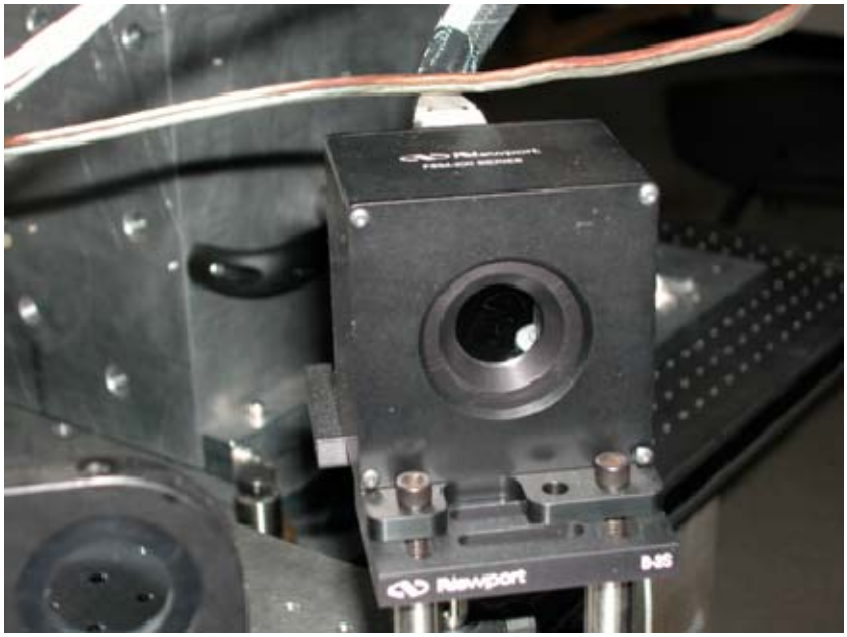

Figure 21 Newport Fast Steering Mirror

A Newport model FSM200 fast steering mirror is used as the receiving fast steering mirror (RFSM) for controlling the disturbances. A two inch mirror is mounted on four voice coils that can steer the mirror in two different axes. The mirror has four BNC inputs and two BNC outputs, with an optional internal closed loop. In these experiments, the mirror was used in open-loop mode. The mirror was given x and y position commands from the computer control system. The two position outputs of the mirror were not utilized in these experiments. The unit has a 1 μrad rms resolution with a control bandwidth of approximately 550 Hz at 100 μrad amplitude. The x and y axes of the Newport mirror are aligned 90° to those of the detectors. One must ensure the mirror is powered on before actuating the inertial shaker to ensure the mirror is not damaged. The specifications for the mirror are found in Appendix C.

D. INERTIAL ACTUATOR

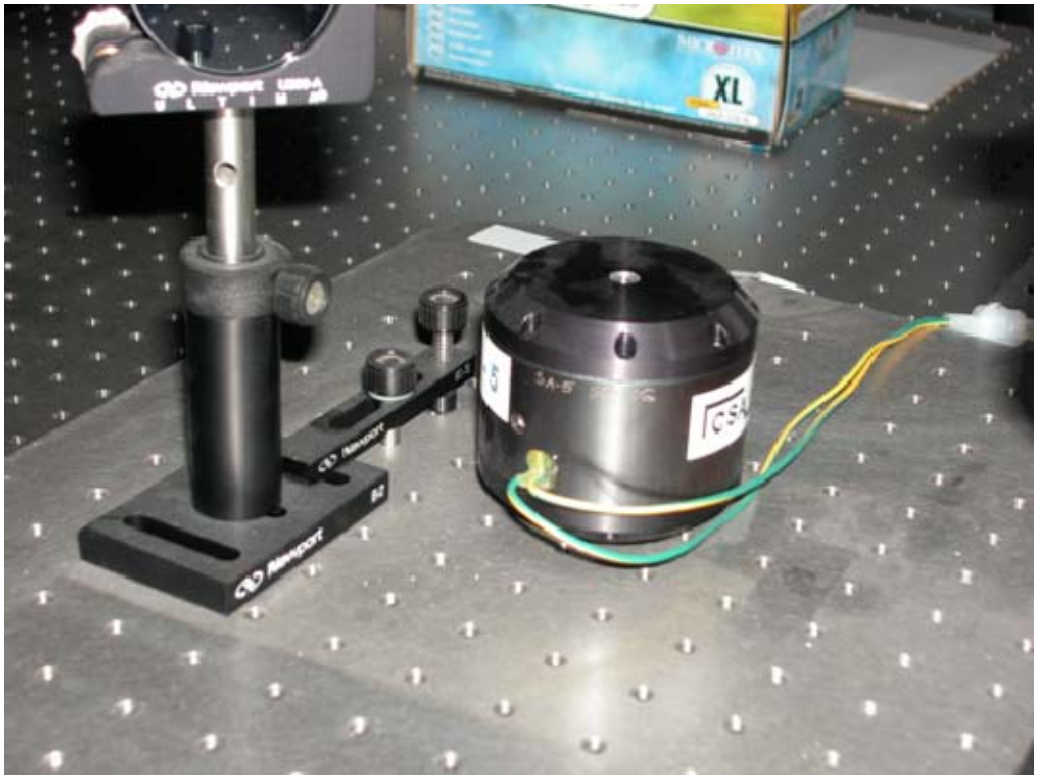

Figure 22 CSA Engineering Inertial Actuator

An CSA Engineering Model SA-5 Inertial Actuator is mounted on the small Newport Vibration Isolation Platform. The inertial actuator exhibits a 40 Hz resonance frequency. The actuator is designed to deliver a force of 5 lbf over a bandwidth of 20 to 1000 Hz. The shaker has an electromagnetic circuit with a moving magnet that delivers force along the cylinder's axis. The inertial actuator was not used in any of the experiments presented in this thesis.

E. VIBRATION ISOLATION PLATFORMS

1. Newport Optical Table

A Newport R4000 Breadboard is mounted on four Newport I-2000 isolators as the base for the LJC Testbed. The table is designed to reduce vibration from the floor when

the table is floated on low pressure air. The isolators do not reduce very low frequency disturbances as shown below in the graphs in Figure 23.

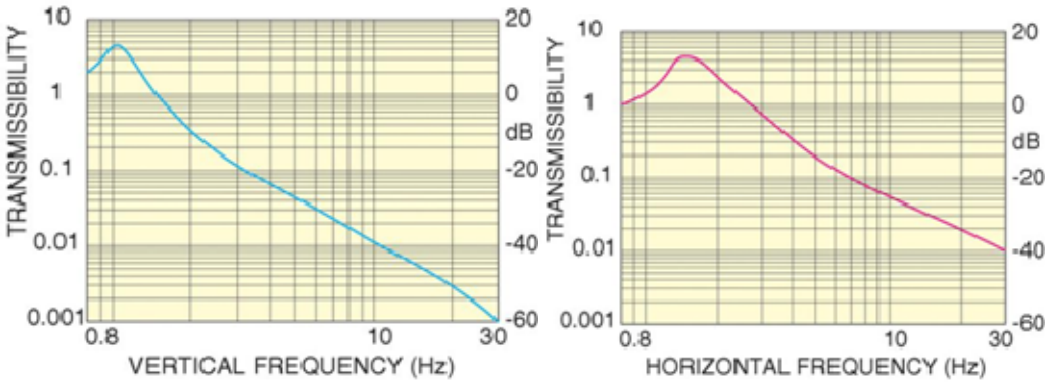

Figure 23 Newport I-2000 Pneumatic Isolator. From [Newport]

2. Newport Vibration Isolation Platform

A Newport Vibration Isolation Platform is mounted on the optical bench. The RFSM and other beam splitters and folding mirrors are mounted on this smaller isolation platform. This setup is designed to isolate the main optical bench from the vibrations from the inertial actuator. The frequency response plots of the platform in Figure 24 show that very little motion is transmitted to the main optical bench above the resonance frequencies of the table. As long as the motion of the table is kept above about 15 Hz, less than a tenth of the motion will be passed on to the main bench. Additionally, the main bench is so much more massive that the small amount of force that the platform does transmit from the 5 lbf shaker will be quite insignificant.

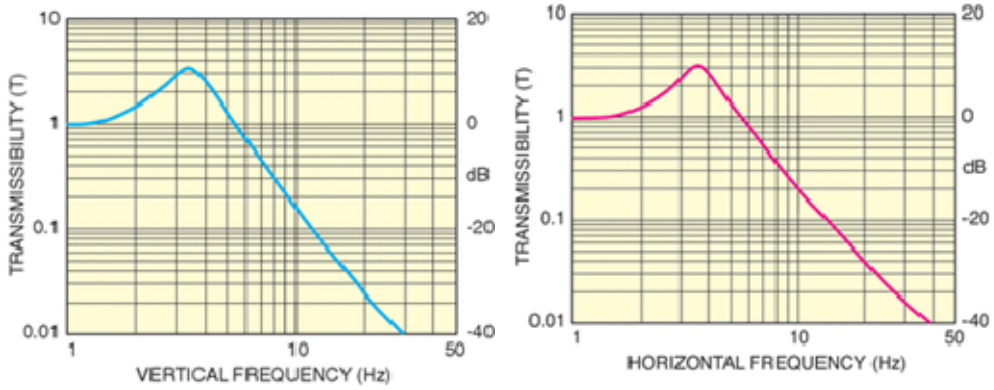

Figure 24 Newport Vibration Isolation Frequency Response. From [Newport]

F. COMPUTER CONTROL SYSTEM AND SOFTWARE

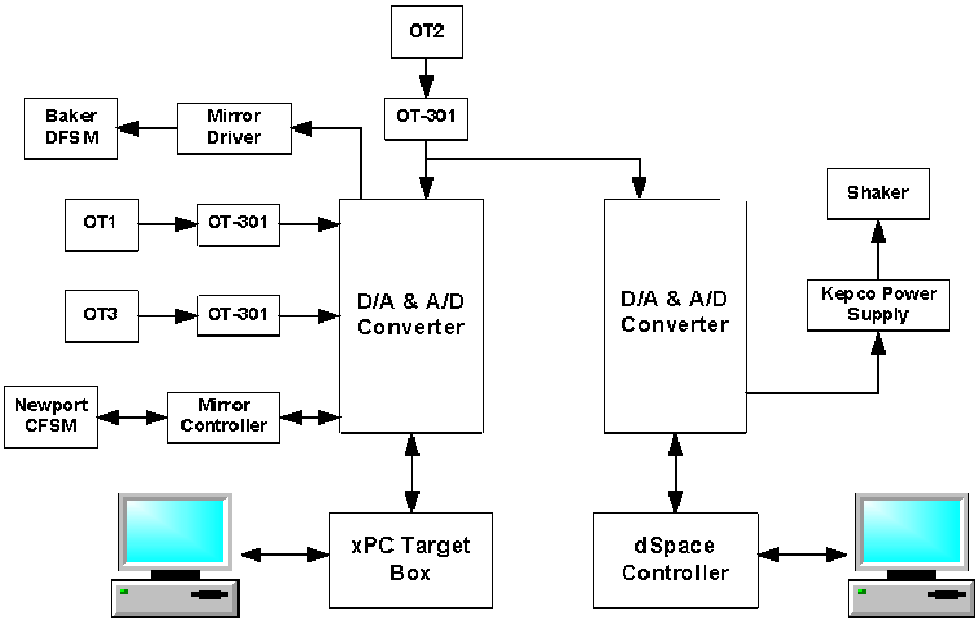

Figure 25 Signal Flow Diagram. After [Watkins 35]

Three computers are used for conducting experiments on the LJC Testbed. The core of the control system is MATLAB version 6.1 release 13 with both SIMULINK and xPC Targetbox from Mathworks. The main controller PC is a 2.66 GHz Dell OPTIPLEX GX260 with 1 Gbyte of RAM. It interfaces with the hardware through the xPC Target Box, which can provide 4 analog outputs and 16 differential inputs. The xPC Target Box controls the disturbance from the Basker DFSM and the correction from the Newport RFSM. The xPC Target Box is a Pentium III with a processing speed of 700 MHz. The signal flow diagram is shown above in Figure 25. The disturbance PC is an Intel Pentium 4 3.2 Ghz computer with 1 Gbyte of RAM. It is used to control the inertial shaker through a dSPACE Controller version 3.3. The versions of software used for the LJC Testbed are listed in Appendix D. Future plans are to update the LJC Testbed to support more computationally complex algorithms such as an order-recursive Recursive Least Square adaptive feedforward controller in lattice filter form.

V. SYSTEM IDENTIFICATION EXPERIMENTS

Accurate mathematical modeling of the Laser Jitter Control (LJC) Testbed is necessary to design effective controllers. The open loop response of the system is necessary for designing a fixed feedback controller and certain adaptive feedforward controllers. The system that needs to be modeled is from the voltage input of the Newport fast steering mirror to the voltage output of the position sensing detector OT2. The mathematical model should capture the frequency response of the system for all frequencies of concern. This experiment is based on rejecting low frequency broadband noise less than 35 Hz. The control mirror will respond at much higher frequencies since the sampling was completed at 2 kHz. There are two inputs and two outputs for this system divided into one input and one output for each axis. Experimental results showed negligible coupling between the two axes of the Newport fast steering mirror. An input to one axis of the mirror yielded less than 1/10 of movement in the other axis for typical amplitudes used in the experiments. Therefore, system identification was performed for each axis separately, assuming they were uncoupled. There are several different methods for completing the system identification.

A. NON-PARAMETRIC FREQUENCY DOMAIN METHOD

Past system identification research on the LJC Testbed is based upon the assumption that the systems behaves as a second order system. Watkins modeled the Newport fast steering mirror as a second order system and the position sensing detector (PSD) as a first order system. The state space variables identified by Watkins were the PSD output, V_p, the angle, θ, of the Newport fast steering mirror, and the angular velocity, $\dot{\theta}$,of the same mirror (Watkins 44). Sugathevan used a second order system for the Newport fast steering mirror and a scalar gain for the detector, using the same first two state variables (Sugathevan 2). The angular velocity of the mirror was estimated using a Kalman estimator. The large bias required by the disturbance fast steering mirror (DFSM) to avoid erratic behavior made using the receiving fast steering mirror's (RFSM)

position output difficult as a state variable. The PSD's response time of 67 μs is much faster than the sampling time used of 0.0005 s, so minimal delay is attributed to the detector.

Non-parametric frequency domain methods of system identification usually consist of exciting the system with a sweeping chirp signal to determine the natural frequency of the system. The damping coefficient can be found by analyzing the response of the system to a step input. These two values are then plugged into a second order transfer function to obtain the mathematical model in transfer function form or state space form. This continuous time model must then be converted to discrete time to use it on a discrete system. The main shortfall of this continuous time method is the assumption that system is a certain order, which may not be correct. MATLAB has made system identification in discrete time very efficient and accurate.

B. PARAMETER ESTIMATION METHOD

The parameter estimation method of system identification consists of exciting the system with a signal of sufficient distinct frequencies and then analyzing the data by using a computer to determine the best model using parametric modeling techniques. Typical signals that can meet this input criterion are filtered Gaussian white noise, a random binary signal, or a chirp sinusoid. Several different algorithms are available for analyzing the data using MATLAB's System Identification Toolbox, such as ARX, ARMAX or State Space (Ljung 418).

1. Experimental Results of System Identification

Each axis of the Newport fast steering mirror was tested individually with a linearly sweeping sinusoid signal from 1 to 1000 Hz for 200 seconds. For simplicity, system identification will only be shown for the y axes. The system was sampled at 2 kHz, with PSD OT2 as the output. A bode magnitude plot was created from the experimental data for a benchmark with which to compare various subspace-based models, as shown below in Figure 26 for the y axis. The Hilbert transform of the voltage output is calculated in one Hertz bins. The magnitude of the voltage gain is found by

dividing the mean of the absolute value of the analytic signal by the input amplitude. This is plotted on a bode magnitude plot as shown below in Figure 26 under *Experimental Data*. Commands from MATLAB's System Identification Toolbox were used as follows and as shown in Appendix E.

The mean of the input and output data was removed. From the bode plot shown in Figure 26, the bandwidth of the open-loop system is approximately 500 Hz for the y axis. Therefore, only the data from the first 120 seconds (up to 800 Hz) was considered. The time delay of the data was found to be 1 sample. MATLAB's *n4sid* function for parametric modeling in state space recommended a third order state space model. This estimate was based on initial conditions of zero and zero disturbance. Each of the three state space variables is unknown for this initial estimate. In order for the state space model to have more physical significance so an integrator can be added to the Linear Quadratic Gaussian (LQG) controller, it is desired to have one of the state space variables be the output of the system, OT2. The grey-box model was constrained additionally to make the discrete C matrix [1 0 0], which realizes the first state variable to be equal to the output if the D matrix is zero, by using the *n4sid* command with the canonical restriction. More flexibility is available in constraining the grey-box model by manipulating a state space model estimate by using the *idss* and *set* functions in MATLAB. The *pem* function can then estimate a revised state space model. Both methods yield similar results, but the canonical constraint was slightly better than restructuring a grey-box model with the *set* function. The second and third state variables of the state space model are not directly measureable, but they may be estimated using a Kalman estimator. This procedure was performed for each axis. This procedure yielded one third order discrete state space model for each axis.

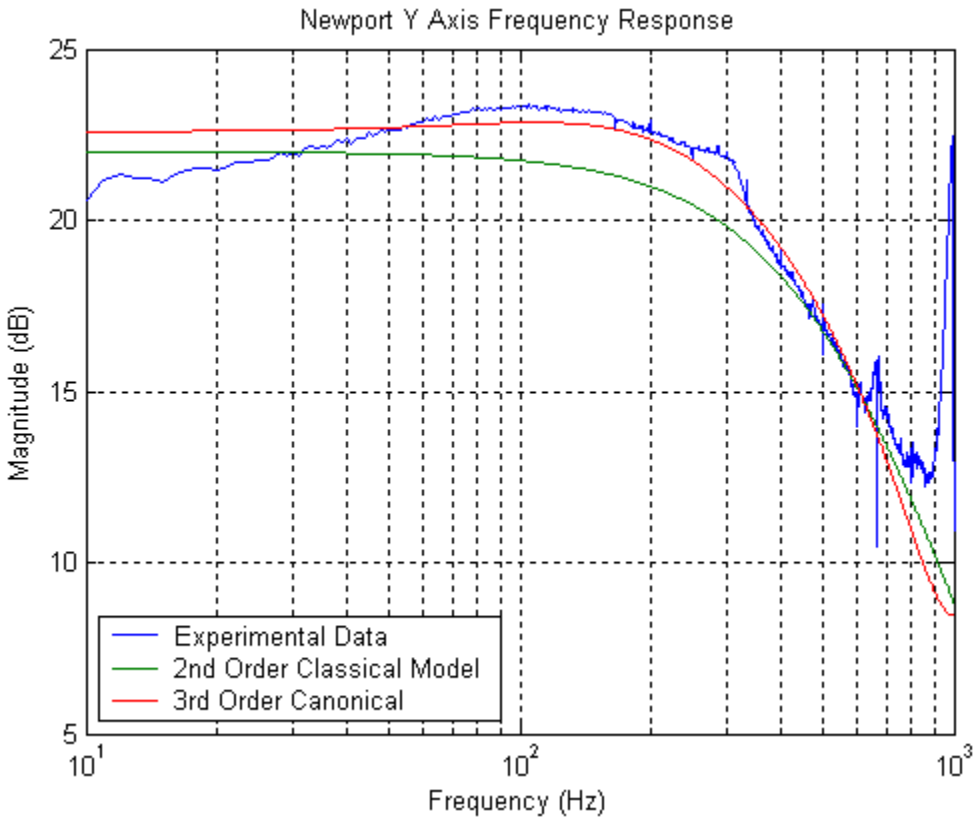

Figure 26 Frequency Response of Open-Loop System Y-Axis

The bode plot of the state space model is shown above in Figure 26 for the y axis. The figure compares Sugathevan's second order model with the third order state space model calculated above. Sugathevan calculated a damping coefficient of 0.95 with natural frequencies of 3708.4 rad/s and 3261.5 rad/s for the x and y axes, respectively (Sugathevan 2).

MATLAB's *compare* function was used to test the fit of the models for the y axis to the sweeping sinusoid data set. The canonical third order state space model and second order classical model had a fit of 71.38% and 46.02%, respectively. A second experimental data set was obtained with a random binary input signal used with a 1 kHz anti-aliasing filter. The performance of the two models was 78% and 71.27% for the canonical third order model and second order classical model, respectively.

The third order discrete state space model calculated for the y axis is shown below. The only known physical state space variable is the first variable, V_{dy}, which is the OT2 detector voltage for the y axis in units of volts. The last two state variables of the canonical model can be estimated using a Kalman estimator.

$$\begin{bmatrix} V_{dy}(k+1) \\ x_2(k+1) \\ x_3(k+1) \end{bmatrix} = \begin{bmatrix} 0 & 1 & 0 \\ 0 & 0 & 1 \\ -0.01 & -0.28 & 1.01 \end{bmatrix} \begin{bmatrix} V_{dy}(k) \\ x_2(k) \\ x_3(k) \end{bmatrix} + \begin{bmatrix} 3.1 \\ 7.9 \\ 2.7 \end{bmatrix} u(k) \tag{5.1}$$

$$V_{dy}(k) = \begin{bmatrix} 1 & 0 & 0 \end{bmatrix} \begin{bmatrix} V_{dy}(k) \\ x_2(k) \\ x_3(k) \end{bmatrix} \tag{5.2}$$

The same procedure was carried out for system identification of the open-loop response of the x axis. The frequency response plot is shown below in Figure 27 for the x axis.

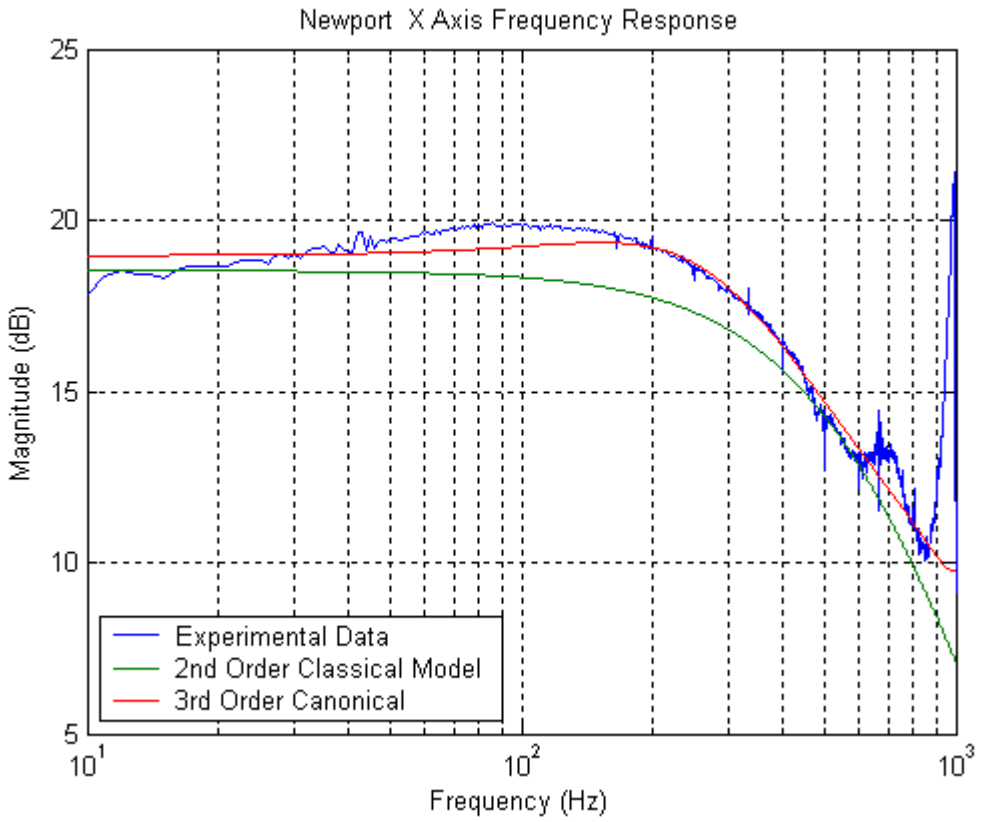

Figure 27 Frequency Response of Open-Loop System X-Axis

Matlab's *compare* function returned 68.05% and 50.33% for the third order canonical and second order classical model, respectively, for the chirp sine input.

The constrained third order state space model for the x axis follows:

$$\begin{bmatrix} V_{dx}(k+1) \\ x_2(k+1) \\ x_3(k+1) \end{bmatrix} = \begin{bmatrix} 0 & 1 & 0 \\ 0 & 0 & 1 \\ -0.12 & 0.12 & 0.40 \end{bmatrix} \begin{bmatrix} V_{dy}(k) \\ x_2(k) \\ x_3(k) \end{bmatrix} + \begin{bmatrix} 2.9 \\ 5.6 \\ 0.49 \end{bmatrix} u(k) \tag{5.3}$$

$$V_{dx}(k) = \begin{bmatrix} 1 & 0 & 0 \end{bmatrix} \begin{bmatrix} V_{dx}(k) \\ x_2(k) \\ x_3(k) \end{bmatrix} \tag{5.4}$$

VI. DISTURBANCE REJECTION EXPERIMENTS ON THE LJC TESTBED

Four different experiments were run on the Laser Jitter (LJC) Testbed to test the controllers under different types of disturbances. Broadband and narrowband disturbances were created with the disturbance fast steering mirror (DFSM). Broadband disturbances were created by filtering the output of the *Band-Limited White Noise* block in *Simulink* with a band pass filter. The band pass filter was designed to pass noise from 4 to 33 Hz. Narrowband noise was created by driving the DFSM with a *Sine Wave* block from *Simulink* at 50 Hz. Vibration from the building and misalignments of the test bed contribute a small amount of additional disturbance. The disturbance for Case 1 is a small low frequency broadband noise from 4 to 33 Hz. Case 2 has a larger broadband disturbance over the same frequency range. Case 3 tests the controllers against a 50 Hz narrowband disturbance. The last experiment, Case 4, has a combination of both narrowband and broadband disturbances.

Each experiment is 10 seconds long sampled at 2 kHz. The disturbance is injected with a random bias from the DFSM at the start of the experiment. The controller then turns on at 4 seconds for the remainder of the data run.

Several measures of effectiveness are analyzed to evaluate the performance of each controller. The Mean Square Error (MSE) is calculated by averaging the square of the error in microns of the laser beam at the detector OT2. The origin of the detector is chosen as the target. The averaging is completed by a moving average filter of the last 200 data points. The MSE is plotted to show the convergence rate of each controller. The MSE starts out quite large due to the initial random bias of the laser beam's position. The standard deviation of the beam is calculated as a measure of jitter reduction for each axis. The input jitter is measured for one second duration at three seconds before the controller turns on. The controlled jitter is calculated from the last one second of data. The mean value of the laser beam's position in nanometers is determined from the last one second of data. And last, the reduction in power spectral density (psd) in decibels at the injected narrowband disturbance frequency of 50 Hz is calculated as a performance

measure. The MATLAB command *pwelch* was used to calculate the power spectral densities using Welch's method. The data was windowed with a 2048 length Hamming Window and a 50 % overlap 2048 length Fast Fourier Transform. The uncorrected psd was calculated from 2^{12} data points, or roughly two seconds of data, starting at 1 second into the data run. The corrected psd was calculated from 2^{12} data points starting from 6 seconds.

A. LQG CONTROLLER

A Linear Quadratic Guassian (LQG) controller was constructed to evaluate the adaptive feedforward control techniques. The weighting matrix **Q** is a zero matrix except for the weight of 1700 corresponding to the integrator state variable. The input weighting matrix **R** was set at 0.1. This combination of weighting was found by trial and error to show the best performance. The voltage output of the detector OT2 was used to measure the first and fourth state variables. The second and third unknown state variables were estimated using a Kalman estimator. The LQG controller and Kalman estimator calculations are shown in Appendix F.

B. DISTURBANCE REJECTION EXPERIMENTS

1. Case 1: Small Broadband Disturbance from DFSM

The disturbance fast steering mirror (DFSM) was driven with a small broadband noise to simulate low frequency disturbances on a ship from 4 to 33 Hz as discussed in Chapter II. The power spectral densities for each axis and the mean square error are plotted as follows. Tabulated data in Table 3 shows the results of additional calculations.

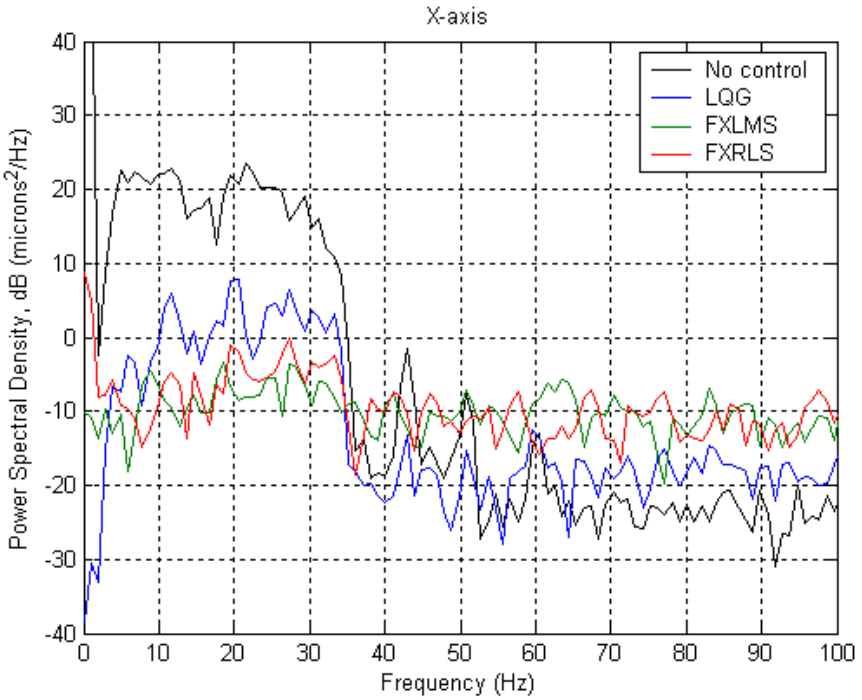

Figure 28 X Axis PSD Case 1, Small Broadband Disturbance

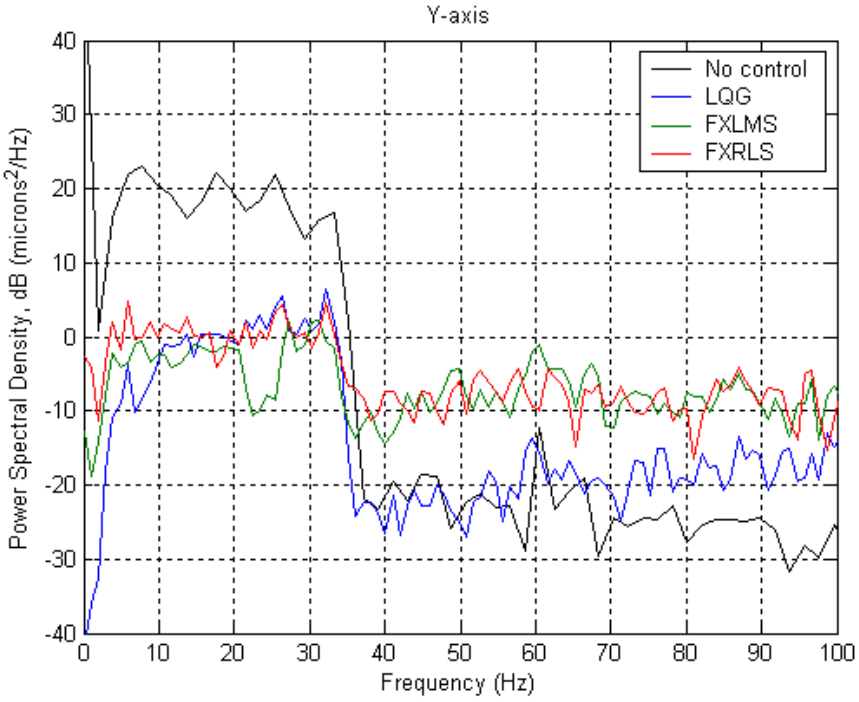

Figure 29 Y Axis PSD Case 1, Small Broadband Disturbance

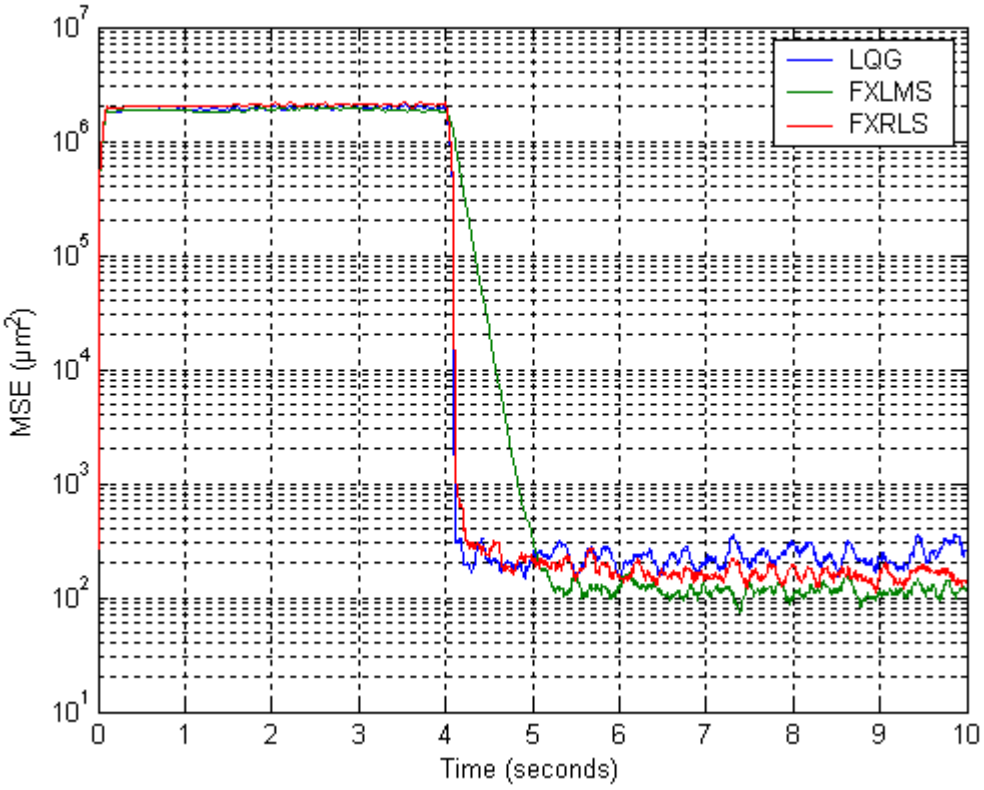

Figure 30 Mean Square Error Case 1, Small Broadband Disturbance

	LQG		FXLMS		FXRLS	
Control Mirror Axis	X axis	Y axis	X axis	Y axis	X axis	Y axis
Input Jitter, St. Dev. (μm)	55.7	57.4	51.4	46.4	55.5	57.5
Controlled Jitter, Std. Dev. (μm)	11	11.6	6.1	8.8	7.1	10.1
% Reduction of Jitter	80.3	79.8	88.1	81	87.3	82.4
# of Stages	n/a	n/a	1	1	10	10
Mean Beam Position Error (nm)	-32.6	168.2	74	-246.3	2467.3	-113.1
MSE at 10 seconds (μm^2)	257.6		109.4		136.8	

Table 3. Case 1 Results, Small Broadband Disturbance

Case 1 shows that all three controllers are effective for this low frequency broadband disturbance. Both the feedback and adaptive feedforward controllers achieved an 80% reduction in jitter. The gain of the output of the Filtered-X least mean square (FXLMS) controller was lowered to provide a lower MSE, but the convergence rate suffers. One stage was found to be optimum for the FXLMS controller for disturbances from the DFSM. The DFSM can only provide disturbance in two axes. The disturbances

show up at each detector at the speed of light with insignificant phase delay. Therefore the FXLMS controller does not need many stages for optimum disturbance rejection. Ten stages were used on the Filtered-X recursive least square (FXRLS) controller. The current hardware setup limits the number of stages that can be used with the FXRLS controller since it is so computationally expensive. A few more stages can be achieved by lowering the sample rate, which is a tradeoff for accuracy. Both adaptive feedforward controllers amplify the higher frequency noise much more than the LQG controller.

2. Case 2: Large Broadband Disturbance from DFSM

A larger broadband disturbance over the same frequency from 4 to 33 Hz was tested to determine the limits of the controllers. The power spectral density plots, MSE plot, and tabulated data follow.

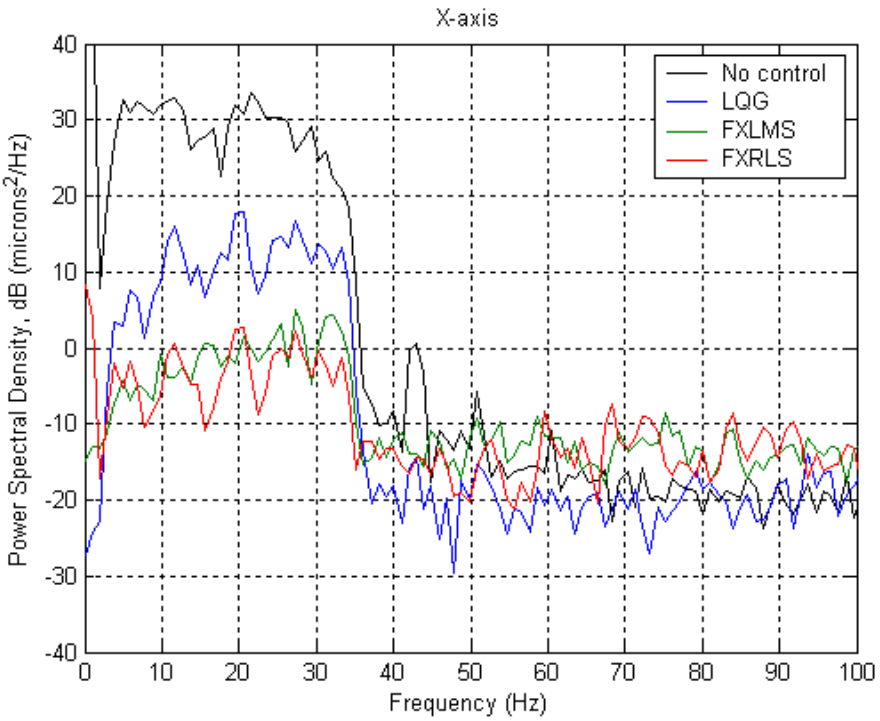

Figure 31 X Axis PSD Case 2, Large Broadband Disturbance

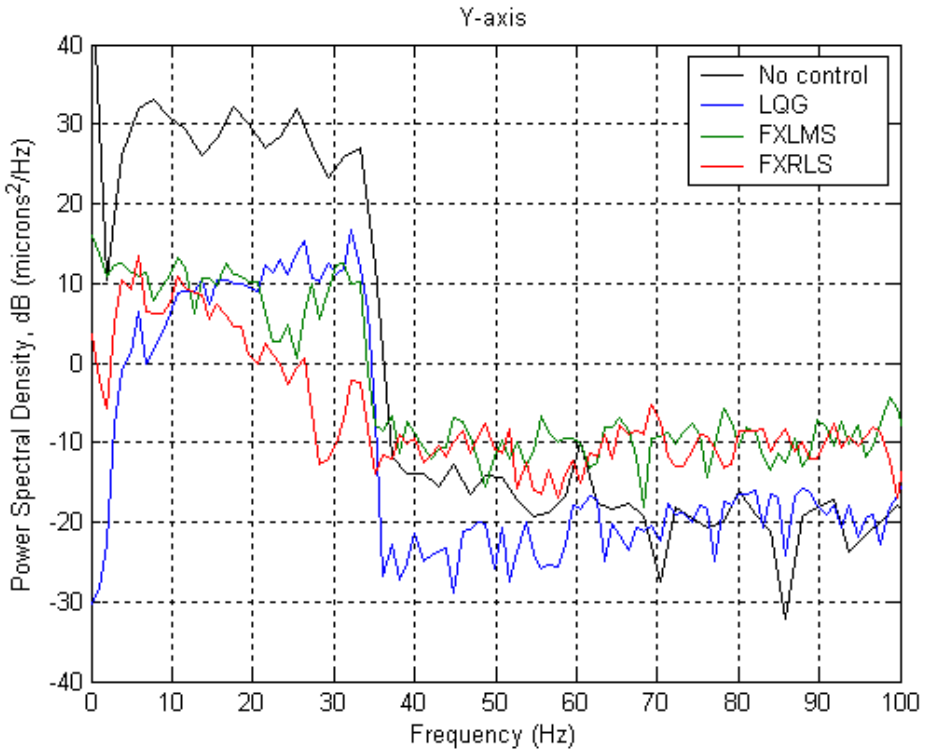

Figure 32 Y Axis PSD Case 2, Large Broadband Disturbance

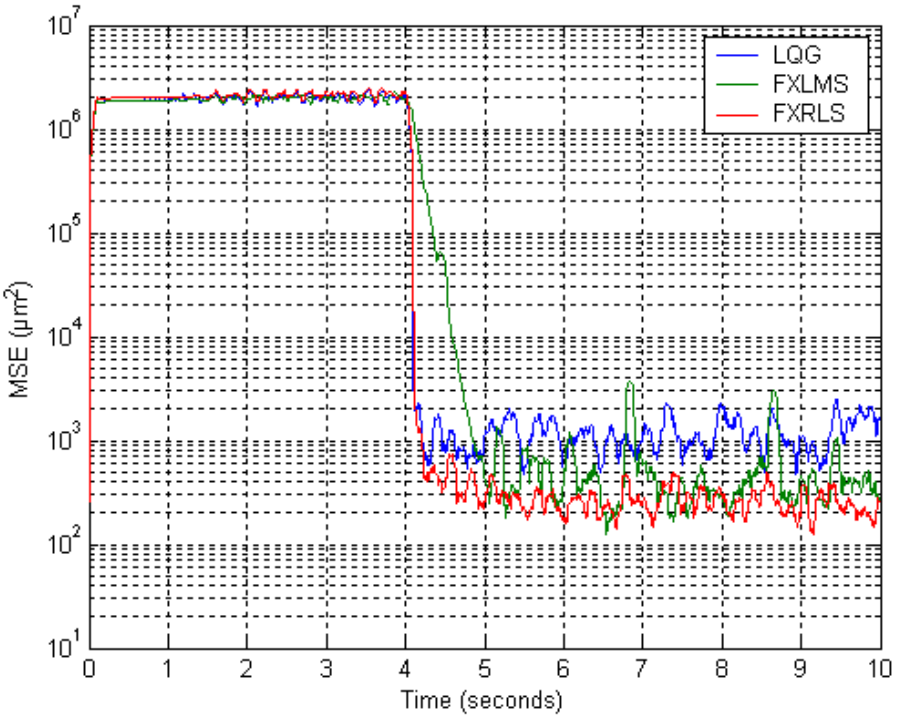

Figure 33 MSE Case 2, Large Broadband Disturbance

	LQG		FXLMS		FXRLS	
Control Mirror Axis	X axis	Y axis	X axis	Y axis	X axis	Y axis
Input Jitter, St. Dev. (μm)	177.4	183.4	165.6	144.4	176.5	183.3
Controlled Jitter, Std. Dev. (μm)	29.6	22.9	8.1	18.0	7.4	13.3
% Reduction of Jitter	83.3	87.5	95.1	87.5	95.8	92.7
# of Stages	n/a	n/a	1	1	10	10
Mean Beam Position Error (nm)	-134.1	514.9	-206.7	-5209.4	2265.0	2383.2
MSE at 10 seconds (μm^2)	1706.8		284.0		267.0	

Table 4. Case 2 Results, Large Broadband Disturbance

The FXRLS adaptive feedforward controller performed the best in jitter reduction under this larger broadband disturbance with a 95.8% and 92.7% reduction in jitter for the X and Y axis, respectively. The mean beam position error is quite large at over two microns for each axis of the FXRLS controller, meaning all of the random bias was not taken out effectively.

3. Case 3: Narrowband Disturbance from DFSM

A 50 Hz narrowband disturbance was injected into each axis using the DFSM. The power spectral density plots for each axis show the LQG controller used both with and without a 50 Hz notch filter. The tabulated data in Table 5 only includes data from the LQG controller with the notch filter.

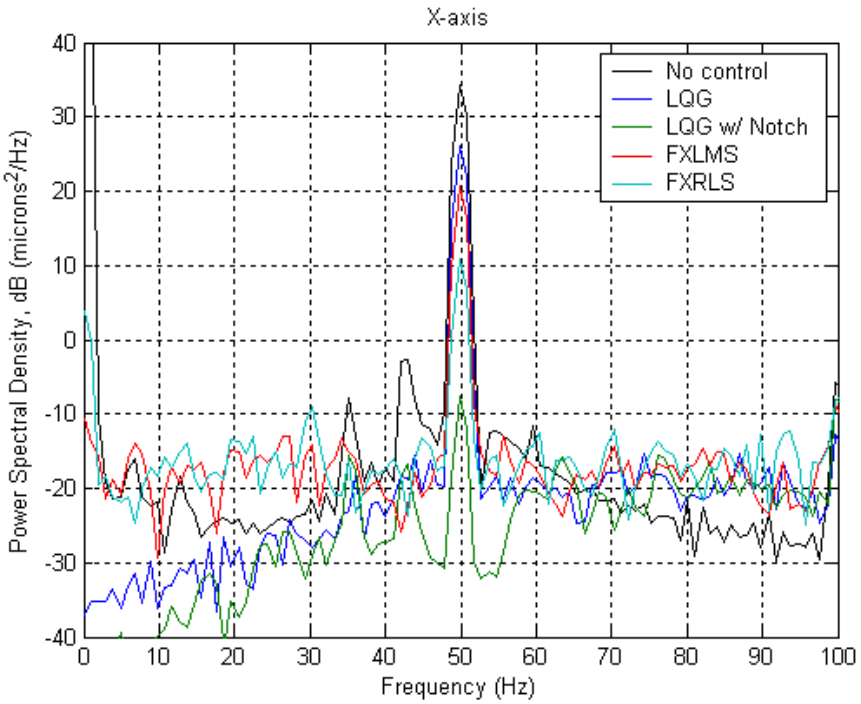

Figure 34 X Axis PSD Case 3, Narrowband Disturbance

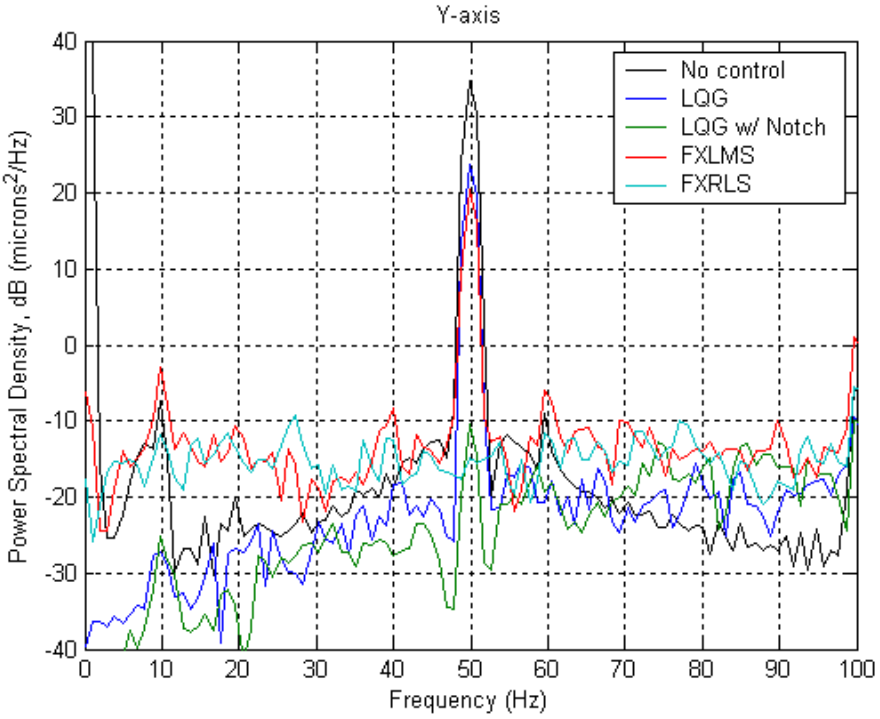

Figure 35 Y Axis PSD Case 3, Narrowband Disturbance

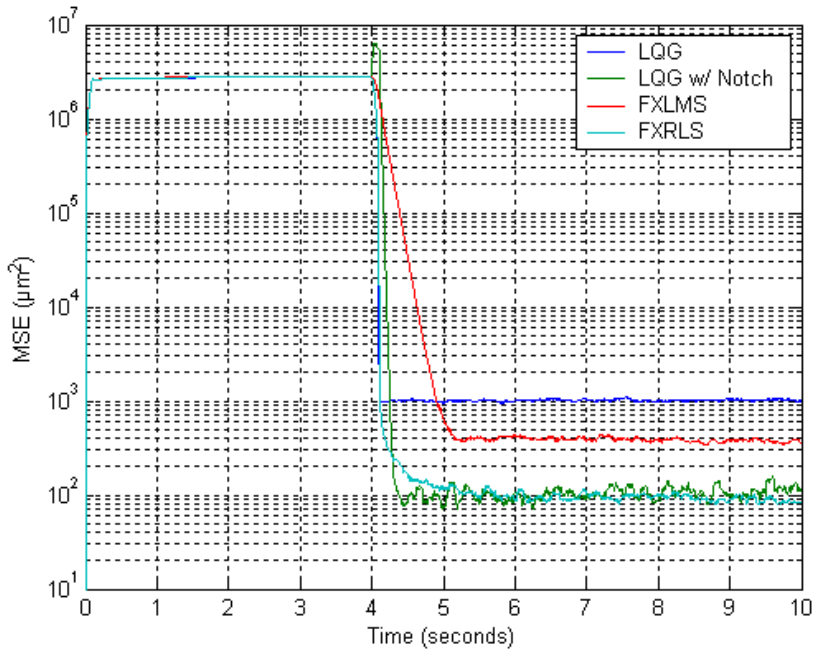

Figure 36 MSE Case 3, Narrowband Disturbance

	LQG w/ Notch Filter		FXLMS		FXRLS	
Control Mirror Axis	X axis	Y axis	X axis	Y axis	X axis	Y axis
Input Jitter, St. Dev. (μm)	62.4	64.9	61.9	65.0	62.2	65.0
Controlled Jitter, Std. Dev. (μm)	5.8	8.9	12.8	14.6	6.7	6.6
% Reduction of Jitter	90.7	86.3	79.4	77.6	89.3	89.8
# of Stages	n/a	n/a	1	1	10	10
Mean Beam Position Error (nm)	2.0	-13.1	-316.8	-600.4	85.7	-28.0
dB Reduction at 50 Hz	42.0	45.2	13.7	14.3	23.5	49.5
MSE at 10 seconds (μm^2)	110.7		360.9		81.0	

Table 5. Case 3 Results, Narrowband Disturbance

The LQG controller with the notch filter performed the best, but only slightly better than FXRLS controller. The notch filter was designed to specifically reject the narrowband disturbance at a known frequency. The FXRLS performed nearly as well with no *a priori* information of the disturbance and achieved a 49.5 dB reduction in psd at 50 Hz in the y axis.

4. Case 4: Narrowband and Broadband Disturbance from DFSM

The last experiment has both a narrowband and broadband disturbance from the DFSM. The power spectral density plots, MSE plot, and tabulated data follow.

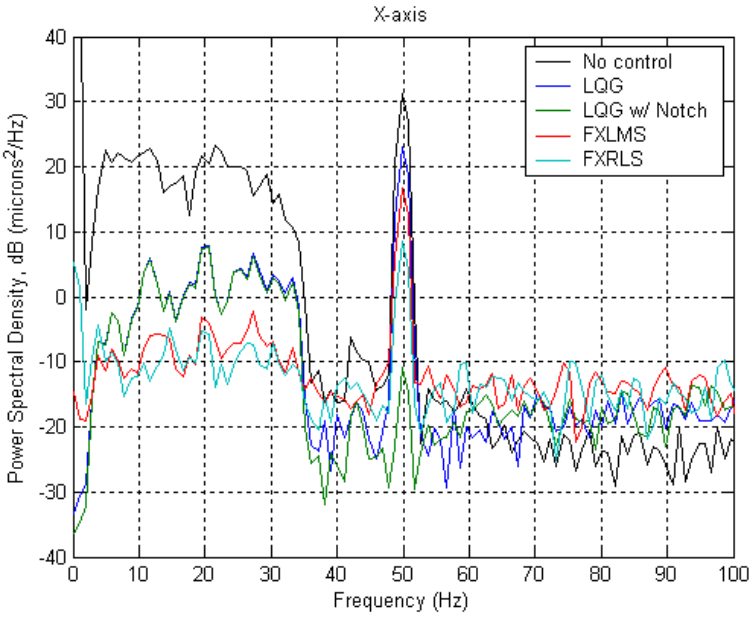

Figure 37 X Axis PSD Case 4, BB and NB Disturbance

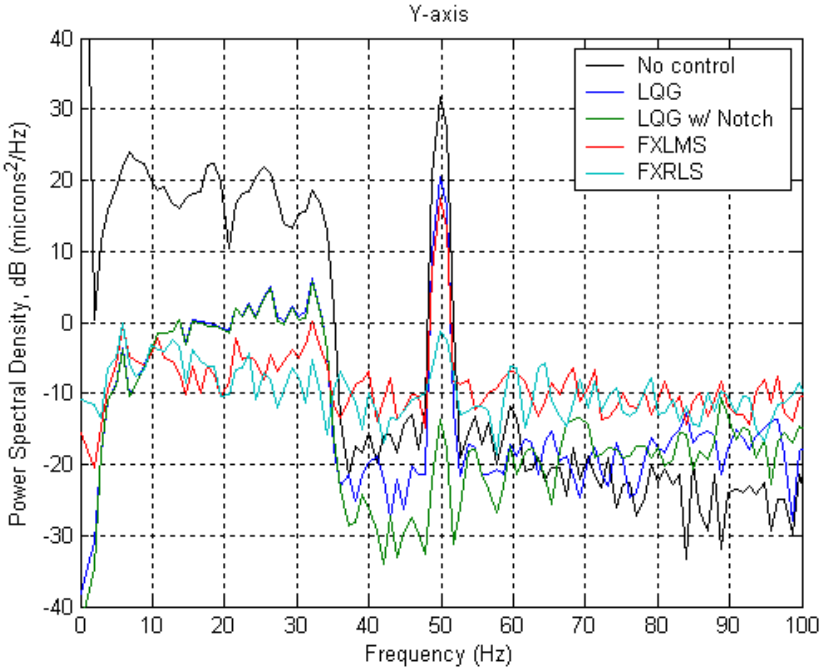

Figure 38 Y Axis PSD Case 4, BB and NB Disturbance

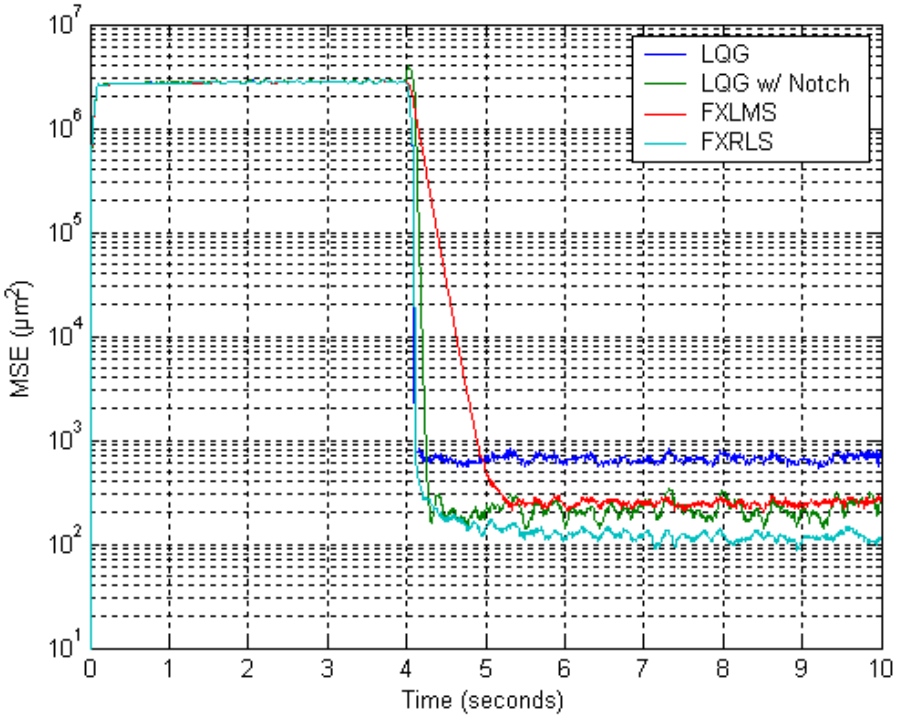

Figure 39 MSE Case 4, NB and BB Disturbance

	LQG w/ Notch Filter		FXLMS		FXRLS	
Control Mirror Axis	X axis	Y axis	X axis	Y axis	X axis	Y axis
Input Jitter, St. Dev. (μm)	69.5	72.9	69.6	72.5	69.4	72.5
Controlled Jitter, Std. Dev. (μm)	10.4	11.1	10.4	12.2	6.8	8.4
% Reduction of Jitter	85.1	84.7	85.1	83.2	90.1	88.5
# of Stages	n/a	n/a	1.0	1.0	10.0	10.0
Mean Beam Position Error (nm)	-52.5	162.5	-64.1	-9.6	1591.7	387.1
dB Reduction at 50 Hz	42.1	45.2	14.4	14.1	22.7	33.0
MSE at 10 seconds (μm^2)	249.4		259.8		117.9	

Table 6. Case 4 Results, NB and BB Disturbance

The FXRLS adaptive feedforward controller performed the best against both disturbances with a MSE of only 117.9 μm^2. One drawback of the FXRLS controller is the residual bias shown by the large mean beam position error. The disturbance has a constant random bias just over 1.6 mm. The FXRLS controller did not use any bias estimator to estimate this large constant error. Therefore, the controller had to

compensate by changing all of the weighting coefficients to try and minimize the error. Adding one additional weight for the bias term would reduce the mean beam position error.

VII. DESIGN RECOMMENDATIONS FOR FREE ELECTRON LASER WEAPON SYSTEM VIBRATION CONTROL

An airplane and a ship are both difficult environments to operate a laser weapon system that demands precise alignment. The Airborne Laser (ABL) and FEL face similar problems regarding vibration and alignment. The ABL beam control technology has overcome many obstacles in vibration control, but the problem is not yet solved. Tests to date have shown that mechanical jitter is a major problem on the ABL. The mechanical jitter will be even worse when the actual high energy laser has been installed on the aircraft due to the disturbances generated by the high energy laser system. The most effective vibration control technique for each system may be different, due to the differences in the operating environment and differences in the laser systems themselves.

A. EXAMPLE VIBRATION CONTROL OF AN OPTICAL BEAM SYSTEM – THE AIRBORNE LASER

The U.S. Air Force Airborne Laser (ABL) is a missile defense weapon system carried in a modified Boeing 747 aircraft. It is designed to destroy airborne missiles by directing energy from a megawatt Chemical Oxygen Iodine Laser (COIL) at an airborne missile. Years of research have produced successful techniques for operating precision lasers on vibrating and moving platforms. The Beam Control function controls the laser beam through the on board optical system and through the atmosphere to the target. Portions of the Beam Control function related to onboard disturbances will be the focus of this discussion. The total jitter budget on the ABL is less than a microradian (Glaese 152).

The ABL employs three separate lasers: a high energy COIL laser, a tracking laser, and a beacon laser. The high energy laser is produced at the rear of the fuselage of the aircraft and travels forward to the fine beam control system mounted on a vibration isolated optical bench. The high energy laser is directed at the target by a nose turret with a 1.5 diameter meter telescope mirror system. The multiple beam tracking laser tracks the target for aiming the high energy laser and provides initial atmospheric disturbance

data. The kilowatt beacon laser irradiates the target in order to provide information on atmospheric aberrations that is utilized by deformable mirrors as part of the beam control system ("ABL YAL 1A").

Beam jitter is controlled on the ABL by a combination of passive isolation, structure design, and active control systems. The beam expander telescope inside the nose turret is attached to an inertial reference transfer unit that directs a laser reference from an inertial reference platform back through the beam train to a sensor on the forward optical bench anti-parallel to the line of sight of the missile. A rear optical bench houses the track and beacon lasers. The beam train and the layout of the ABL is shown below in Figure 40 and Figure 41.

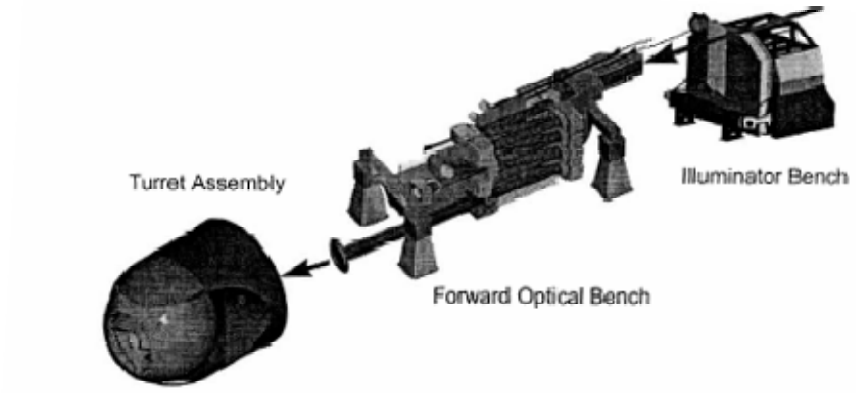

Figure 40 ABL Beam Train. From [Kenchner 12]

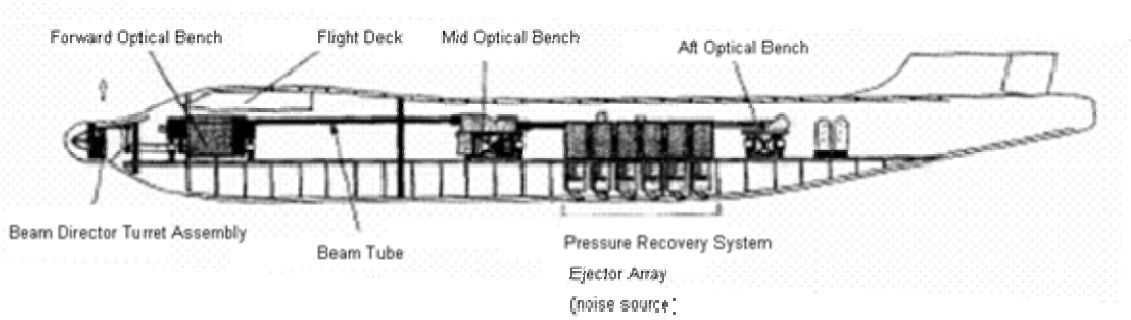

Figure 41 ABL Component Diagram. From [Glaese 152]

The aft and mid optical benches are isolated from the airframe by very soft air springs. Each of the eight air springs for each bench is a hybrid pneumatic-electromagnetic actuator. The eight actuators on each bench maintain the two benches in alignment in six degrees of freedom by referencing a central bench target. Five degrees of motion are measured optically, while the 6th fore-aft measurement between the two benches is made by transducers integral to the actuator mounts (Kienholz).

Closed loops between the forward and rear optical benches maintain beam alignment using a pair of fast steering mirrors for each loop. The active control system has 8 control loops as shown below in Figure 42 (Kelchner 13).

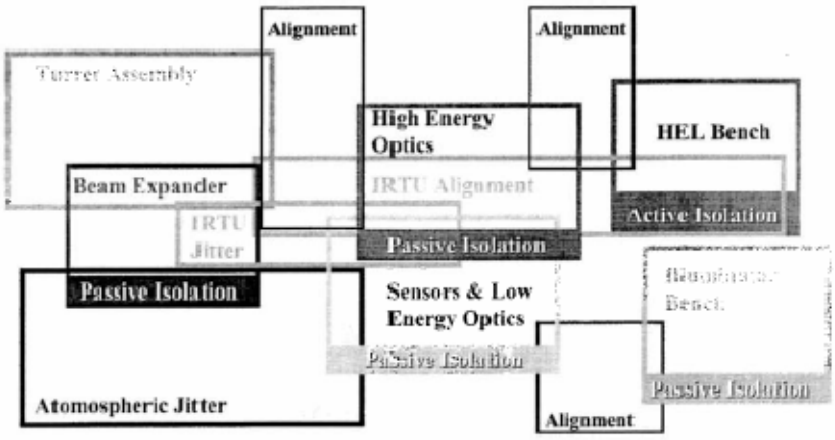

Figure 42 ABL Jitter Control Architecture. From [Kelchner 12]

Four major sources of jitter contribute to vibration on an airborne laser: mechanical vibrations from airplane hardware, air turbulence that causes the plane to flex and a bumpy ride, vibrations induced by airflow around the turret, and noise and vibrations from operating the laser (Duffner 137-138). One of the important lessons learned on the first airborne laser project, called the Airborne Laser Laboratory (ALL), was the degrading effects of acoustically induced jitter primarily produced by the pressure recovery system of the COIL laser and the high amplitude acoustic fields produced by air flow against the turret (Glaese 151-152).

B. COMPARISON OF AIRBORNE LASER AND FREE ELECTRON LASER DESIGN

Mass restrictions, proximity to vibration sources, proximity to loud noise sources, and air turbulence are major challenges for the ABL. A FEL on a large ship allows much more design flexibility on where to place the weapon with respect to noise and vibration sources. Additional mass can be very beneficial as a passive design tool to dampen vibration and especially acoustic noise. The airframe of the ABL can flex under turbulence. A ship also flexes due to seas, but additional mass and reinforcements over the length of the optical cavity of the FEL could add much needed stiffness. Fortunately, any additional mass needed for vibration isolation purposes would be quite insignificant compared to the mass of the ship.

Air turbulence on the beam director on a ship will be quite minimal compared to that on the turret of the ABL. Additionally, a FEL on a ship will not have a loud source of acoustic disturbances inherent to producing the laser such as the ABL's pressure recovery system. Therefore, acoustic noise will be a minor concern for disturbance of a FEL on a ship.

The total jitter requirement for the ABL of one microradian is the same as the jitter requirement for the FEL plant on a ship. The proposed length of 20 meters for the FEL optical cavity is very close to the approximate 50 foot distance between the aft and mid optical benches for the high energy beam.

On the other hand, a ship at sea is constantly moving in a large amplitude cyclic motion at low frequencies, while an airplane can be quite stable when not maneuvering. Sea spray on the beam director optics and more atmospheric aberrations at lower altitudes below the clouds also present a challenge for laser beam control for the FEL on a ship.

The ABL program has come a long way in addressing jitter caused by mechanical and acoustical disturbances. The jury is still out on whether the jitter requirements will be met once the high energy laser is installed and operational. There may be other ways to improve vibration isolation, and so to lower the jitter, that are not used on the ABL.

C. DESIGN RECOMMENDATIONS FOR THE VIBRATION CONTROL OF AN FEL ON A SHIP

Beam jitter will have to be controlled on the ship by a combination of passive isolation, structure design, and active control systems. Design recommendations presented herein will be focused primarily on the most critical part of the FEL plant, optical beam control in the optical cavity.

Usually jitter control refers to controlling the angular deviation of a laser. Over long distances, such as for a satellite relay, the translational movement of the beam is quite inconsequential compared to the effect of a small error in angular position. On the FEL plant, both angular and translational errors of the optical and electron beam will be significant over the 20 meter optical path between mirrors. Translational movement of the mirrors and undulator in phase and at the same amplitude wouldn't be a problem, but relative motion between these critical components would cause misalignment. For this reason, active translational position control is necessary to maintain alignment.

One difficult design dilemma is balancing both passive isolation and multiple optically aligned benches. Passive isolation could drastically reduce high frequency disturbances. But the movement of the ship such as ship's roll could cause misalignment of the multiple benches if the passive isolation is too "soft." The amount of passive isolation will have to be balanced with the ability of the active alignment system to maintain alignment. A two stage passive isolation would be even more effective at reducing the transmissibility of the support structure disturbances. Passive isolation causes amplification of low frequency vibration at the resonance of the isolator, as was shown in Figure 5.

There are primarily two design options for mounting the fast steering mirrors of the optical beam. The first option includes using three individual actively aligned benches that are mounted on hybrid pneumatic-electromagnetic actuators, similar to those used on the ABL aft and mid benches. This approach is similar to that used on the ABL. The center bench would support the undulator. Two fast steering mirrors would be

mounted on each of the two end optical benches. The second option is to mount these three optical benches on top of a single integrated platform that is passively isolated from the ship.

The second option of one single integrated platform has potential of better jitter reduction than the jitter suppression design used on the ABL. The single integrated platform would need to be approximately 20 meters longs. The rigidity of the platform would minimize the displacement required of the active actuators. The distance between the mirrors would be easier to control with the single platform. Another advantage is that the platform would lower the frequencies of the disturbances to where active control would be more effective. CSA Engineering has built a large platform mounted on passive air isolations that is 30 by 82 feet for a similar purpose. The giant platform's first mode doesn't occur until 12 Hz. The large passively mounted platform would need to have lateral active actuators to control the platform's lateral motion when the ship rolls, yaws, or pitches (Kienholz).

The three optical benches would then be mounted on the single integrated platform on six or eight hybrid pneumatic-electromagnetic actuators. The three benches could be maintained in alignment in six degrees of freedom in relation to a reference laser beam inside a vacuum to minimize atmospheric aberrations. One fast steering mirror on each bench is for reflecting and controlling the high energy laser. A smaller reference fast steering mirror is mounted rigidly to the same support as the primary fast steering mirror on each bench. The reference fast steering mirrors will be controlled with adaptive feedforward controllers to steer an additional reference laser to minimize the mean square error of the laser's position at optical detectors on the undulator optical bench.

Several important items should be considered concerning vibration control for choosing the location of the FEL plant on a ship. The FEL plant should be placed away from any loud running equipment. The weapon should be installed on the deck of the ship in a location where no prominent structural vibration modes are apparent. The three critical benches should be installed at anti-nodes of vibration. A mirror mounted on a vibration node would have small translation but higher angular displacement, which is a

larger source of jitter. Finding such a site would require an extensive vibration survey for potential installation sites. This survey would also reveal the area of a ship that has the lowest structural vibrations. The deck of the ship should be reinforced to minimize flexing or bending of the base of the FEL plant.

Knowledge of the disturbances should be exploited as much as possible by using adaptive feedforward controllers. References of the vibration used in this manner can contribute to much higher jitter rejection than a traditional or adaptive feedback system can provide. Fortunately, the atmospheric disturbances in the optical cavity will be very small if it is in a vacuum, so most disturbances can be measured. Many types of measurements can be made to provide a reference. Possible references include the following: optical angular and translational position detectors, accelerometers, gyros, and laser inferometers. Optical references should be used when possible since they provide the most accurate position information. An Inertial Reference Unit could provide a very stable reference laser beam to optically align the benches.

There will be several sources of vibration that affect the FEL on a ship. An adaptive filter used for an adaptive feedforward controller will best be implemented in lattice form to accommodate multiple references and even cross-axis coupling. An order-recursive adaptive filter would allow fast convergence with a small number of stages for coarse jitter control before transitioning to a large number of stages for precise jitter control. If the disturbances on a ship are found to be relatively invariant, the weights of the adaptive feedforward controller can be fixed in a simple feedforward controller to ease the computational burden.

THIS PAGE INTENTIONALLY LEFT BLANK

VIII. CONCLUSIONS

A. SUMMARY OF RESULTS

The research described in this thesis was conducted to analyze the feasibility of using a Free Electron Laser on a naval ship in such a difficult vibration environment. The effects of vibration on the Free Electron Laser and possible methods of both passive and active jitter control were discussed. Vibration experiments were performed on the Laser Jitter Control Testbed at the Naval Postgraduate School to test several types of vibration controllers.

Experiments on the Laser Jitter Control Testbed were focused on three different controllers: a Linear Quadratic Gaussian (LQG) feedback controller, a Filtered-X least mean square (FXLMS) adaptive feedforward controller, and a Filtered-X recursive least square (FXRLS) adaptive feedforward controller. A Newport fast steering mirror was controlled to reduce jitter induced by a disturbance fast steering mirror. The disturbance fast steering mirror was driven with a 4 to 33 Hz broadband disturbance, a 50 Hz narrowband disturbance, or a combination of the two.

A parametric system identification technique was used to accurately model the system in order to design an effective Linear Quadratic Gaussian controller. The LQG controller worked best for a small broadband disturbance, but performed poorly for the narrowband disturbance. A notch filter was employed to effectively attenuate the 50 Hz narrowband disturbance. Since the LQG controller is not adaptive, the controller will be less effective if the system is prone to change during operation. The notch filter used with an LQG controller will not work as designed if the frequency of the narrowband disturbance changes.

With the exception of the fixed notch filter used for a narrowband disturbance at a known frequency, the adaptive feedforward controllers performed better than the fixed feedback LQG controller. The disturbances injected with the fast steering mirror were measured with an optical detector and used as a reference in the adaptive feedforward controllers. A one stage FXLMS adaptive feedforward controller was quite effective at

correcting the simple jitter induced by the disturbance fast steering mirror. An FXLMS controller is easy to implement and provides better results than the LQG controller. The Filtered-X recursive least square (FXRLS) adaptive feedforward controller with 15 stages was found to be the most effective to correct a combination of both broadband and narrowband disturbances. The FXRLS controller results in a 33 dB decrease in jitter caused by a 50 Hz narrowband vibration and an 89% improvement in low frequency broadband jitter experienced by the optical beam. The FXRLS controller's algorithm is computationally complex to implement due to the large number of calculations required on the order of the number of stages squared. The FXRLS controller has a distinct advantage over the FXLMS controller for narrowband disturbances.

B. CONCLUSIONS

The changing vibration environment on a ship is very harsh. The tight tolerance for the optical beam of a Free Electron Laser of 1 μrad is a formidable specification to meet. The FXRLS adaptive feedforward controller is recommended for this difficult application of a Free Electron Laser on a ship to maintain mirror alignment in the optical cavity that employs a co-linear optical reference beam.

The Free Electron Laser on a ship will experience much lower acoustic noise than the Airborne Laser due to much lower air turbulence on the turret and the absence of a loud pressure recovery system. Even so, this doesn't ensure that FEL operation on a ship is feasible. The Airborne Laser Program's struggle with mechanical jitter shows that mechanical jitter design must be given priority starting from the initial phases of the design process.

C. SUGGESTIONS FOR FOLLOW-ON RESEARCH

As a result of the research done on the Laser Jitter Control Testbed and the FEL, several areas have arisen that require further study. These include the following:

- Modify the FXRLS adaptive feedforward filter to estimate and reduce the bias more effectively. The FXRLS controller provided the best jitter rejection in this research, but did not remove all of the random bias of the disturbance.

- Updating the Laser Jitter Control Testbed would allow research on more computationally complex algorithms. This would provide the ability to test the FXRLS controller against a more difficult disturbance such as from an inertial actuator without locking up the computer. A higher number of stages is needed for the controller to capture all of the phase delays of the disturbance.

- Employ an order-recursive FXRLS filter in lattice form on the Laser Jitter Control Testbed. This would allow more than one reference signal and cross-coupling of control axes of the controlling fast steering mirror.

- Conduct a detailed, multiple-point, linear and angular vibration survey of a prospective area for FEL installation on an underway ship. Measurements using a portable low power laser and an optical detector of a vibrating deck in several locations over the length of 20 meters would provide very useful information on the relative phase and amplitude of disturbances.

THIS PAGE INTENTIONALLY LEFT BLANK

APPENDIX A: TRIAXIAL ACCELEROMETER CALIBRATION CERTIFICATES

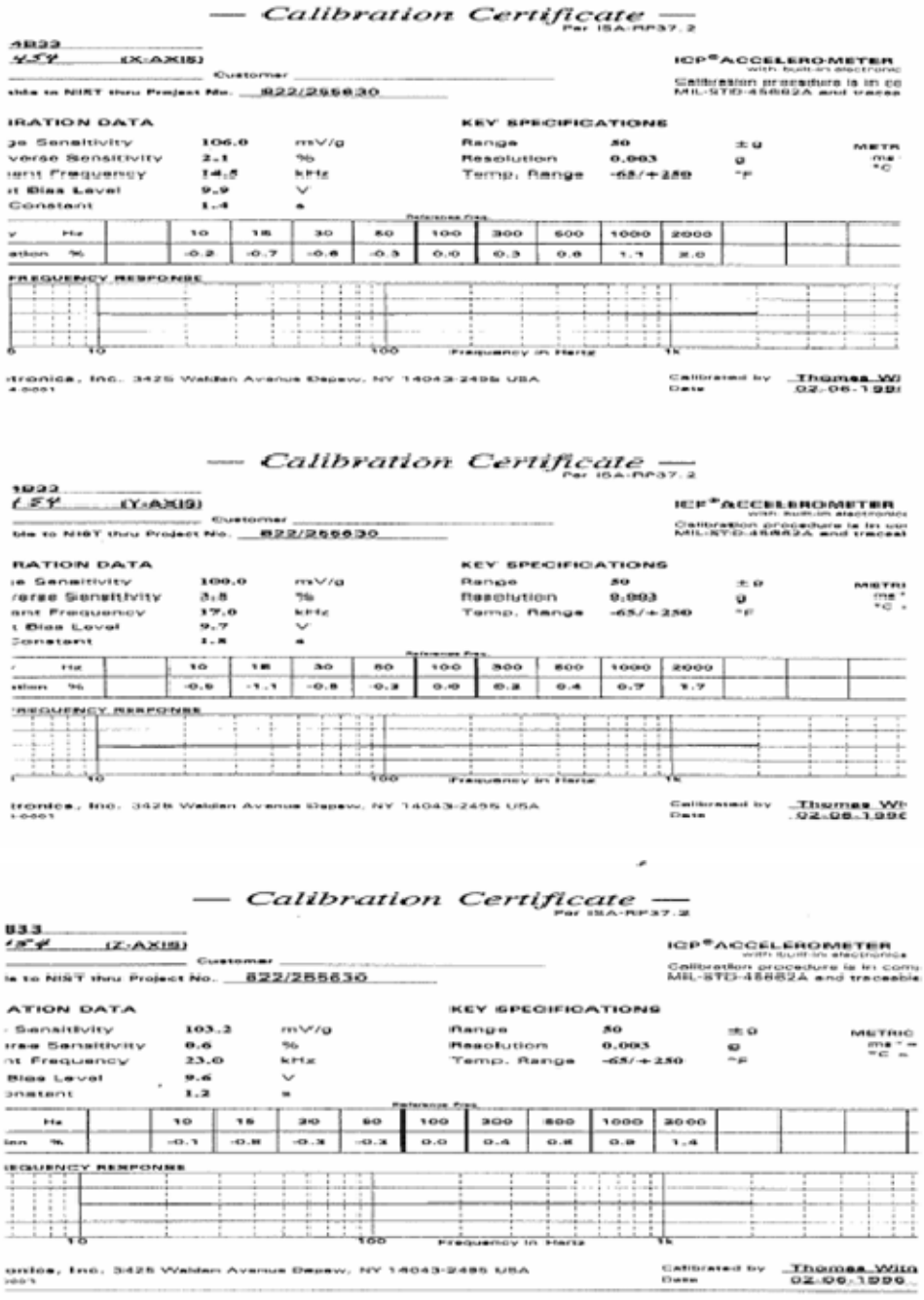

— Calibration Certificate —

Per ISA-RP37.2

4833

(X-AXIS)

Customer

ICP® ACCELEROMETER

with built-in electronics

Calibration procedure is in co

MIL-STD-45662A and traceab

822/255630

IRATION DATA

ge Sensitivity	106.0	mV/g
verse Sensitivity	2.1	%
ural Frequency	14.5	kHz
t Bias Level	9.9	V
Constant	1.4	s

KEY SPECIFICATIONS

Range	50	±g	METR
Resolution	0.003	g	m/s²
Temp. Range	-65/+250	°F	°C

Reference Freq.

Hz		10	15	30	50	100	300	500	1000	2000			
ation %		-0.2	-0.7	-0.6	-0.3	0.0	0.3	0.8	1.1	2.0			

FREQUENCY RESPONSE

tronics, Inc. 3425 Walden Avenue Depew, NY 14043-2495 USA

Calibrated by Thomas Wi

Date 02-06-199

— Calibration Certificate —

Per ISA-RP37.2

4833

(Y-AXIS)

Customer

ICP® ACCELEROMETER

with built-in electronics

Calibration procedure is in con

MIL-STD-45662A and traceat

822/255630

RATION DATA

ge Sensitivity	100.0	mV/g
verse Sensitivity	3.8	%
ural Frequency	17.0	kHz
t Bias Level	9.7	V
Constant	1.5	s

KEY SPECIFICATIONS

Range	50	±g	METRI
Resolution	0.003	g	m/s²
Temp. Range	-65/+250	°F	°C

Reference Freq.

Hz		10	15	30	50	100	300	500	1000	2000			
ation %		-0.5	-1.1	-0.8	-0.3	0.0	0.2	0.4	0.7	1.7			

REQUENCY RESPONSE

tronics, Inc. 3425 Walden Avenue Depew, NY 14043-2495 USA

Calibrated by Thomas Wi

Date 02-06-199

— Calibration Certificate —

Per ISA-RP37.2

833

(Z-AXIS)

Customer

ICP® ACCELEROMETER

with built-in electronics

Calibration procedure is in com

MIL-STD-45662A and traceable

822/255630

ATION DATA

Sensitivity	103.2	mV/g
rse Sensitivity	0.6	%
t Frequency	23.0	kHz
Bias Level	9.6	V
onstant	1.2	s

KEY SPECIFICATIONS

Range	50	±g	METRIC
Resolution	0.003	g	m/s² =
Temp. Range	-65/+250	°F	°C =

Reference Freq.

Hz		10	15	30	50	100	300	500	1000	2000			
tion %		-0.1	-0.8	-0.3	-0.2	0.0	0.4	0.6	0.8	1.4			

EQUENCY RESPONSE

onics, Inc. 3425 Walden Avenue Depew, NY 14043-2495 USA

Calibrated by Thomas Wilh

Date 02/06/1996

Figure 43 Triaxial Accelerometer Calibration Certificates

THIS PAGE INTENTIONALLY LEFT BLANK

APPENDIX B: SAMPLE MATLAB CODE FOR CALCULATION OF DISPLACEMENT FOR LINEAR ACCELEROMETERS

```
% file for importing psd vs. frequency and plotting
% created by Brett Bateman 3/28/07
%--------------------------------------------------------------------
% constants
xsensitivity=0.106;  %V/g  provided by manufacturer
ysensitivity=0.100;  %V/g
zsensitivity=0.1032;  %V/g
g=9.81;   %m/s^2
%--------------------------------------------------------------------
%Import and Calculate
s=importdata('H:\Thesis\vibrationlab\filename.txt');   %import 2 column data
frequency=s(:,1);   %select 1st column data
psdlvoltspk=s(:,2);      %select 2nd column of data
psdvoltspk=10.^(psdlvoltspk/10); %converts from dB
psdvoltsrms=psdvoltspk*.5;
psd=psdvoltsrms/(zsensitivity^2)*g^2;  %converts using sensitivity
psddisplacement=psd./(2*3.14*frequency).^4;
totaldisplacementmicrons=(0.5*sum(psddisplacement)*10^6)^0.5  %from 0.5 Hz bands
dispmicrons=(0.5*sum(psddisplacement(2:800, 1))*10^6)^0.5 %1-400 Hz sum
```

THIS PAGE INTENTIONALLY LEFT BLANK

APPENDIX C: EQUIPMENT SPECIFICATIONS

A. ON-TRAK POSITION SENSING DETECTOR

Model	Active Area mm	Responsivity @ 940 nm A/W	Dark Current nA		Noise Current pA/Hz$^{1/2}$		Capacitance pF@15V	
			Typ.	Max	Typ.	Max	Typ.	Max
2L10SP	10.0 x 10.0	0.63	100	500	1.3	2.5	90	110

Rise Time µs 10-90% 15V		Reverse Bias V			Detector Resistance (kΩ)			Thermal Drift ppm/C°		Position Non-Linearity ±%	
Typ.	Max	Min	Typ.	Max	Min	Typ.	Max	Typ.	Max	Typ.	Max
.40	.80	5	15	20	7	10	16	40	200	0.3	0.8

Table 7. On-Trak Position Sensing Detector Specifications. After ["Position Sensing Modules"]

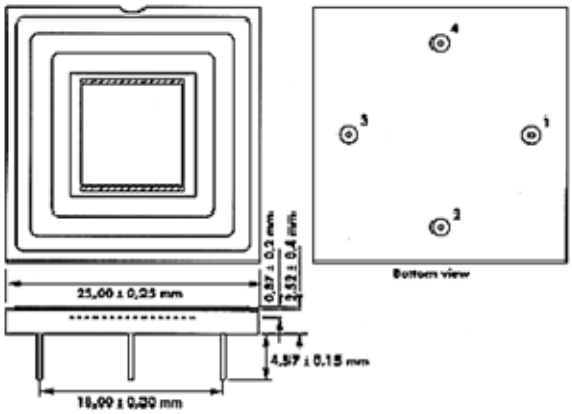

Figure 44 On-Trak Position Sensing Module Diagram. From ["Position Sensing Modules"]

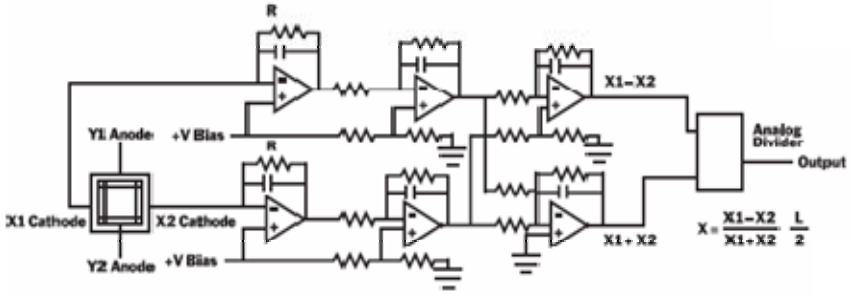

Figure 45 On-Trak Typical Operating Circuit. From ["Position Sensing Modules"]

THIS PAGE INTENTIONALLY LEFT BLANK

B. BAKER STEERING MIRROR

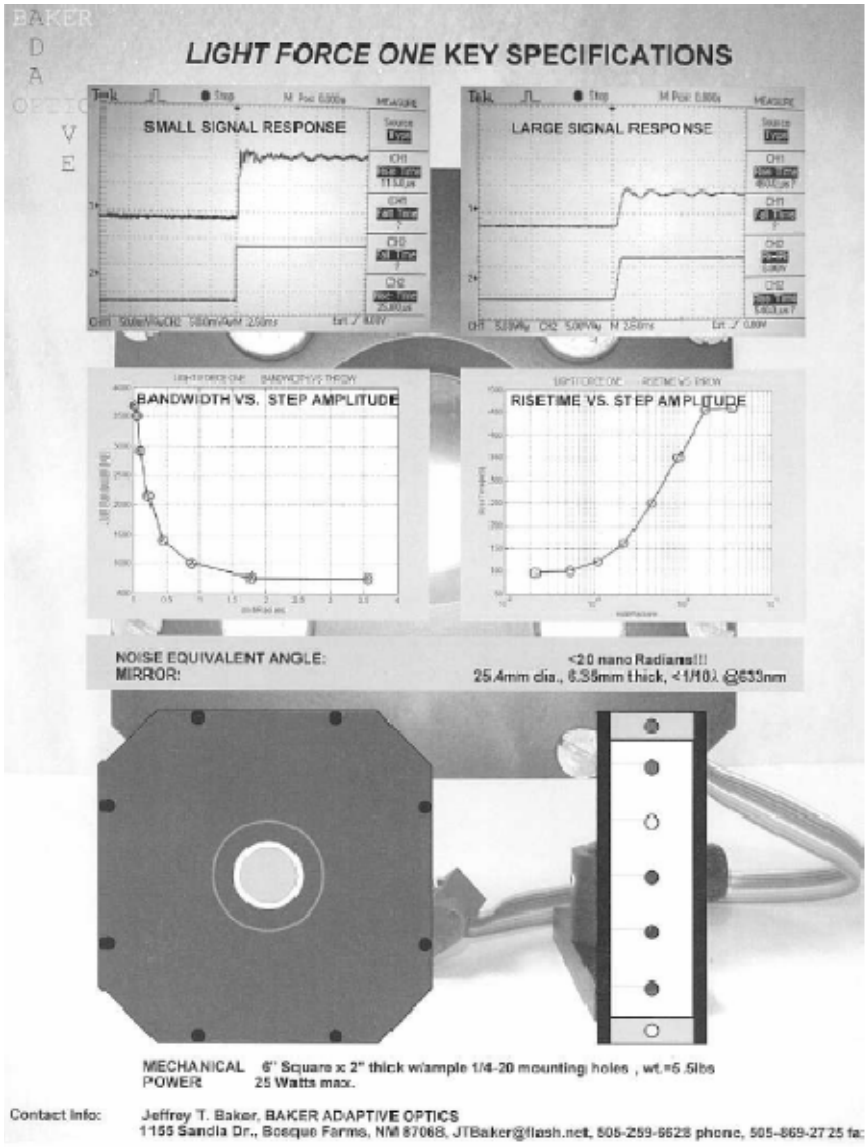

Figure 46 Baker Fast Steering Mirror Specifications. From [Watkins 131]

C. NEWPORT FAST STEERING MIRROR

Number of Axes	2 (tip-tilt)
Angular Range from ±10 V	±26.2 mrad (± 1.5°), Mechanical[4]
Resolution	≤1 µrad rms, Mechanical[1]
Repeatability	≤3 µrad rms, Mechanical[1]
Accuracy From ±26.2 mrad, 25°C[1,2]	≤0.262 mrad (0.015°), Mechanical[1]
Linearity From ±26.2 mrad, 25°C[1,2]	≤1.0%
Peak Angular Velocity	≥2.5 rad/sec, Mechanical[1]
Peak Angular Acceleration	≥900 rad/sec², Mechanical[3]
Closed-Loop Amplitude Bandwidth[2] (-3 dB)	≥550 Hz at 100 µrad amplitude Optional: ≥750 Hz at 100 µrad amplitude
Closed-Loop Phase Bandwidth[2] (60° lag)	≥300 Hz at 100 µrad amplitude
Gain Margin	≥10 dB
Phase Margin	≥45°
Response Flatness[2]	Peaking ≤3 dB
Small Angle Step Response for Steps < 250 µrad, Mechanical[2]	
Rise Time to 90%	≤3.5 msec
Settling Time to 5%	≤5.0 msec
Large Angle Step Response for 26.2 mrad Steps, Mechanical[2]	
Rise Time to 90%	≤3.5 msec
Settling Time to 5%	≤12 msec
Cross-axis Coupling, Static	≤0.1%
Cross-axis Coupling, Dynamic	≤0.1%
Powered Null Offset (Closed-Loop)	±1 mrad, Mechanical[1]
Noise Equivalent Angle (1 Hz to 10 kHz)	≤3 µrad rms
Resolution of Local Position Sensor	≤0.5 µrad
Quiescent Power at FSM Assembly	≤5 W at any angle ±26.2 mrad
Operating Temperature Range[2]	0 to 50°C (32 to 122°F)
Storage Temperature Range	-20 to 55°C (-4 to 131°F)
Warm-up Time for Mirror Stability[2] at 25°C	≤10 minutes
Mirror Thermal Drift[2]	≤5 µrad/°C, Mechanical[1]
Optical Axis Location without base	1.5 in. (38.1 mm) High, Centered Left-to-Right
Mass with base	1.1 lb (0.5 kg)
Envelope without base	3.0 × 3.0 × 2.3 in. [w × h × d] (76.2 × 76.2 × 58.7 mm)
Interconnect Cable Length	9.8 ft (3 m)

Figure 47 Newport Fast Steering Mirror Specifications. From [Watkins 129]

APPENDIX D: SOFTWARE VERSIONS

Software	Version
MATLAB	6.5 R 13
SIMULINK	5.0 R13
xPC Targetbox	2.0 R13+
RealTime Workshop	5.0 R13
dSPACE	Release 3.3
DSP Blockset	5.0 R13.0.1
Control System Toolbox	5.2 R13.0.1
Windows XP	Professional Version 2002 Service Pack 2

Table 8. Software Versions

THIS PAGE INTENTIONALLY LEFT BLANK

APPENDIX E: SYSTEM IDENTIFICATION CODE

```
%System identification using subspace-based method
%
%import data
%-------------------------------------------------------------------------
z=iddata(oo(:,ot2x),oo(:,newyin),0.0005);
zd=detrend(z);
ze=zd(1:320000);  %data to analyze from 1 to 800 Hz
impulse(ze,'sd',3);  %shows delay with 3 standard deviations
%-------------------------------------------------------------------------
%constrained state space model estimate in canonical form
m3canony=n4sid(ze,3,'ss','can','DisturbanceModel','Zero');
%-------------------------------------------------------------------------
%Constrain to grey-box model
mi = idss([1, 1, 0;-1,-.1,.4;0,.27, .6],[.06;0;-0.02],[80,0,0],0,[0;0;0],[0;0;0],'Ts',0.0005);
As = [NaN,NaN,NaN;NaN,NaN,NaN;NaN,NaN,NaN];
Bs = [NaN;NaN;NaN];
Cs = [1,0,0];
Ds=0;
Ks = [0;0;0];
x0s = [0;0;0];
set(mi,'As',As,'Bs',Bs,'Cs',Cs,'Ds',Ds,'Ks',Ks,'X0s',x0s);
%-------------------------------------------------------------------------
%estimate grey-box state space model
m3gy=pem(ze,mi)
%-------------------------------------------------------------------------
%experimental bode magnitude plot
volts=oo(:,ot2x);
input=0.02;  %magnitude of chirp signal in volts to DFSM
amplitude=zeros(1000,1);
magnitude=zeros(1000,1);
N=1000; %# of bins
for i=1:N
   h=hilbert(detrend(volts(400*(i-1)+1:i*400)));
   amplitude(i)=mean(abs(h));
   magnitude(i)=amplitude(i)/input;
   frequency(i)=i;
end
magnitudeb=magnitude(10:1000);%pick off 10 to 1000 Hz data
frequencyb=frequency(10:1000);

%magnitude calculation of models
transfer=tf(m3canony);
```

```
frequency=1:1:1000;
z=exp(j*2*pi*frequency*Ts);
numerator=3.103*z.^2+4.741*z-4.476;
denominator=z.^3-1.014*z.^2+0.2779*z-0.01381;
dBy3canon=20*log10(abs(numerator))-20*log10(abs(denominator));

%Second order model
s=j*2*pi*frequency;
ky=12.59; %DC Gain
wy=3261.5; %natural frequency (rad/s)
lambday=0.95; %damping coefficient
Ay=[0 1;-wy^2 -2*lambday*wy];
By=[0;-wy^2];
Cy=[-ky 0];
Dy=[0];
modely2=ss(Ay,By,Cy,Dy);
[num,den]=ss2tf(Ay,By,Cy,Dy);

numerator=num(3);
denominator=den(1)*s.^2+den(2)*s+den(3);

dBy2=20*log10(abs(numerator))-20*log10(abs(denominator));

figure(1)
semilogx(frequencyb,20*log10(magnitudeb),frequency,dBy2,frequency,dBy3canon)
axis([10 1000 5 25])
xlabel('Frequency (Hz)')
ylabel('Magnitude (dB)')
legend('Experimental Data','2nd Order Classical Model','3rd Order Canonical',3)
title('Newport Y Axis Frequency Response')
grid on
%--------------------------------------------------------------------------------
figure(2)
compare(ze,modely2,m3canony)
```

APPENDIX F: LQG AND KALMAN ESTIMATOR CALCULATIONS

```
%   this program calculates LQG and Kalman Estimator parameters
%   for decoupled 2 axis, 2 input, 2 output system
%   in discrete time

Ts=0.0005;  %sampling time 2 kHz

load m3canonx;  %load model from system identication for each axis
load m3canony;

%theta x
%-------------------------------------------------------------
m3ax=m3canonx;
Ax=m3ax.a;
Bx=m3ax.b;
Cx=m3ax.c;
Dx=m3ax.d;
systemx=ss(Ax,Bx,Cx,Dx,Ts);

%add a fourth state, an integrator
A_augx=[Ax zeros(3,1);-Cx*Ts 1];
B_augx=[Bx;0];
C_augx=[Cx 0];
D_augx=0;

%linear quadratic regulator
Qx=eye(4);  %define weighting matrices
Qx(2,2)=0;
Qx(1,1)=0;
Qx(3,3)=0;
Qx(4,4)=1700;
Rx=0.1;
[Kx,S1x,E1x]=DLQR(A_augx,B_augx,Qx,Rx); %calculate gains

%Compute kalman estimator
Qn = 1e-3;  Nn=0;
Rn=1.797e-6;
Gn=[0.01;0.1;0.01];

Plantx = ss(Ax,[Bx Gn],Cx,0,Ts,'inputname',{'u' 'w'},'outputname','y');
[KESTX,L,P,M,Z] = KALMAN(Plantx,Qn,Rn,Nn);
   Akx=KESTX.a;
```

```
   Bkx=KESTX.b;
   Ckx=KESTX.c;
   Dkx=KESTX.d;

%theta y
%-------------------------------------------------
m3ay=m3canony;
Ay=m3ay.a;
By=m3ay.b;
Cy=m3ay.c;
Dy=m3ay.d;

%add a fourth state, an integrator
A_augy=[Ay zeros(3,1);-Cy*Ts 1];
B_augy=[By;0];
C_augy=[Cy 0];
D_augy=0;

%linear quadratic regulator
Qy=eye(4);
Qy(2,2)=0;
Qy(1,1)=0;
Qy(3,3)=0;
Qy(4,4)=1700;
Ry=0.1;
[Ky,S1y,E1y]=DLQR(A_augy,B_augy,Qy,Ry);

%Compute kalman estimator
Qn = 1e-3;  Nn=0;
Rn=1.797e-6;
Gn=[0.01;0.1;0.01];

Planty = ss(Ay,[By Gn],Cy,0,Ts,'inputname',{'u' 'w'},'outputname','y');
[KESTY,L,P,M,Z] = KALMAN(Planty,Qn,Rn,Nn);
   Aky=KESTY.a;
   Bky=KESTY.b;
   Cky=KESTY.c;
   Dky=KESTY.d;
```

LIST OF REFERENCES

"ABL YAL 1A Airborne Laser, USA." airforce-technology.com. Accessed on 2 Nov. 2007 <http://www.airforce-technology.com/projects/abl/>.

Allen, Charles A., III. "Integrating the FEL on an All-Electric Ship." MS thesis. Naval Postgraduate School, 2007.

Allgaier, Gregory G. "The Shipboard Employment of a Free Electron Laser System." MS thesis. Naval Postgraduate School, 2003.

Bendat, Julius S. and Allan G. Piersol. Engineering Applications of Correlation and Spectral Analysis. 2nd Edition. New York: John Wiley & Sons, Inc., 1993.

Beranek, Leo L. and Istvan L. Ver'. Noise and Vibration Control Engineering: Principles and Applications. 2nd Edition. New Jersey: John Wiley & Sons, Inc., 2006.

Billman, Kenneth W., Bruce A. Horwitz and Paul L. Shattuck. "Airborne Laser System Common Path/Common Mode Design Approach." Proceedings of SPIE 3706 (1999): 196-203.

Colson, William B. Personal Interview. 7 Nov. 2007.

Duffner, Robert W. Airborne Laser: Bullets of Light. New York: Plenum Trade, 1997.

Fiorani, Fulvia M. "Active Mirror Alignment for Free Electron Lasers." MS thesis. Naval Postgraduate School, 2002.

Glaese, Roger M., Eric H. Anderson and Paul C. Janzen. "Active Suppression of Acoustically Induced Jitter for the Airborne Laser." Proceedings of SPIE 4034 (2000): 151-164.

Kelchner, Bryan L. and Ronald Dauk. "ABL Beam Control Segment." Proceedings of SPIE 3381 (1998): 8-13.

Kienholz, David A. Personal Interview. 2 Nov. 2007.

Kuo, Sen M. and Dennis R. Morgan. Active Noise Control Systems: Algorithms and DSP Implementations. John Wiley & Sons, Inc., 1996.

Ljung, Lennart. System Identification: Theory for the User. Second Edition. New Jersey: Prentice Hall PTR, 1999.

Newport. Newport Corporation. Accessed on 5 Nov. 2007. <http://www.newport.com/>.

Ogata, Katshuhiko. Modern Control Engineering. Fourth Edition. New Jersey: Prentice Hall, 2002.

PCB Piezotronics Inc. PCB Group Inc. 7 Nov. 2007. < http://www.pcb.com/>.

"Position Sensing Modules." On-Trak Photonics, Inc. Accessed on 5 Nov. 2007. <http://www.on-trak.com/pdfs/PSM.pdf>.

Stanford Research Systems. Model SR785 Dynamic Signal Analyzer. California: Stanford Research Systems, Inc., 1998.

Sugathevan, Suranthiran and Brij Agrawal. "Optical Laser Pointing and Jitter Suppression Using Adaptive and Feedback Control Methods." Proceedings of Beam Control Conference, Directed Energy Professional Society, Monterey, CA, March 21-24, 2006.

United States. Department of Defense. ANSI S2.25-2004. "Guide for the Measurement, Reporting, and Evaluation of Hull and Superstructure Vibration in Ships."

United States. Department of Defense. MIL-STD-167-1A. "Department of Defense Test Method Standard: Mechanical Vibrations of Shipboard Equipment." 2 Nov. 2005.

Watkins, Joseph R. "The Adaptive Control of Optical Beam Jitter." Diss. Naval Postgraduate School, 2004.

INITIAL DISTRIBUTION LIST

1. Defense Technical Information Center
   Ft. Belvoir, Virginia

2. Dudley Knox Library
   Naval Postgraduate School
   Monterey, California

3. Physics Department
   Naval Postgraduate School
   Monterey, California

4. Professor Brij Agrawal
   Naval Postgraduate School
   Monterey, California

5. Professor Steven R. Baker
   Naval Postgraduate School
   Monterey, California

6. LT Brett E. Bateman, USN
   United States Naval Submarine School
   Groton, Connecticut

7. Professor William B. Colson
   Naval Postgraduate School
   Monterey, California

8. Dr. Hyungjoo Yoon
   Naval Postgraduate School
   Monterey, California